Structure, superconductivity, and magnetism in $Rb_{1-x}Fe_{1.6}Se_{2-z}S_z$

D. Croitori,[1] I. Filippova,[1] V. Kravtsov,[1] A. Günther,[2] S. Widmann,[2] D. Reuter,[2] H.-A. Krug von Nidda,[2] J. Deisenhofer,[2] A. Loidl,[2] and V. Tsurkan[1,2,*]

[1]*Institute of Applied Physics, MD-2028 Chisinau, Republic of Moldova*

[2]*Experimental Physics V, Center for Electronic Correlations and Magnetism, University of Augsburg, 86135 Augsburg, Germany*

(Received 5 September 2019; revised manuscript received 3 February 2020; accepted 7 February 2020; published 26 February 2020)

We report on single-crystal growth, stoichiometry, structure and basic characterization of $Rb_{1-x}Fe_{2-y}Se_{2-z}S_z$ crystals where Se is substituted by S. The temperature and magnetic field dependence of magnetic and thermodynamic properties of all samples was studied by differential-scanning calorimetry, magnetic susceptibility, electrical conductivity, and specific heat. The experimental results are discussed within a T-z phase diagram, which includes vacancy-ordered and vacancy-disordered antiferromagnetic (AFM), superconducting (SC), and nonsuperconducting phases. The structural study reveals change in the local environment of the Fe tetrahedrons depending on substitution: a reduction of the Fe-Fe and Fe-Ch(chalcogen) bond lengths and a tendency for six out- of eight bond angles to approach values realizing a regular tetrahedron and hence, suggesting a reduction of structural distortions with substitution. With increasing substitution, a nonmonotonic decrease of the superconducting transition temperature T_c was observed; the SC state disappears at a substitution level above $z = 1.2$. The SC state coexists with the AFM state that persists in all samples independent of substitution. The transition temperature into the AFM state, T_N, decreases gradually with increasing substitution indicating a weakening of the AFM interactions. The AFM phase exhibits an iron-vacancy-ordered structure below the structural transition temperature T_s. T_s shows a nonmonotonous variation: a decrease with increasing z up to 1.3, followed by an increase on further increasing z. The electronic specific heat reveals a significant reduction of the anomaly at the SC transition temperature indicating a reduction of the density of states at the Fermi energy and a weakening of the electronic correlations that can explain the suppression of the superconductivity with substitution.

DOI: 10.1103/PhysRevB.101.054516

I. INTRODUCTION

In recent years, alkali-metal intercalated iron selenides $A_{1-x}Fe_{2-y}Se_2$ (with $A = K$, Rb, Cs) have attracted significant attention due to their unusual structural and electronic properties [1–5]. They show a fascinating coexistence of an insulating antiferromagnetic (AFM) majority phase $A_{0.8}Fe_{1.6}Se_2$ with iron-vacancy-ordered superstructure (245 phase) and stripes of a minority metallic iron-vacancy-free $A_{1-x}Fe_2Se_2$ phase (122 phase), which becomes superconducting (SC) below a critical temperature T_c of 30 K. Despite numerous studies of intercalated Fe chalcogenides using various local and macroscopic techniques, the interrelation between the AFM and SC phases is far from being well understood (see Refs. [1–6] and references therein). The heterogeneous nature of $A_{1-x}Fe_{2-y}Se_2$ crystals complicates their investigation and analysis and impedes elucidation of the intrinsic behavior.

Currently, there exists a common agreement that in $A_{1-x}Fe_{2-y}Se_2$, the minority phase is responsible for SC properties. This phase is a derivative of the nonmagnetic FeSe that superconducts below 8 K in bulk [7], while for monolayers a possible T_c of 65–100 K was deduced from singular experiments [8,9]. It should be noted that the T_c of the order of 28–33 K [10–18] for $A_{1-x}Fe_{2-y}Se_2$ family is close to T_c of 37 K for bulk FeSe under high pressure [19,20]. In FeSe, the T_c increases from 8 K at ambient pressure to 27 K at 1.5 GPa [21]. This increase is accompanied by a strong increase of AFM fluctuations that are present above T_c [22]. The significantly enhanced T_c by external pressure suggests a connection of the SC parameters and local structural environment of Fe atoms pointing to an important role of structural changes with pressure which influences the electronic properties [20].

In intercalated $A_{1-x}Fe_{2-y}Se_2$ superconductors, the interplay of lattice and electronic degrees of freedom and the response of T_c to pressure are much more complex. For example, in $K_{0.8}Fe_{1.7}Se_2$ crystals, the critical temperature T_c gradually decreases with applied pressure up to 9.2 GPa, while above this pressure the SC state is fully suppressed being accompanied by a structural transition from the Fe-vacancy ordered $I4/m$ to a vacancy disordered $I4/mmm$ phase [23]. Further studies of $K_{0.8}Fe_{1.7}Se_2$ and $Tl_{0.4}Rb_{0.4}Fe_{1.67}Se_2$ discovered a second SC phase emerging between 11.5 and 13 GPa with a T_c of 48 K, significantly higher than the initial T_c [24]. In $Rb_{1-x}Fe_{2-y}Se_2$, full suppression of the SC state was found at a pressure of 6 GPa [25,26]. However, in contrast to $K_{0.8}Fe_{1.7}Se_2$, in SC $Rb_{0.8}Fe_2Se_2$ no structural transformations of the AFM phase up to 15.6 GPa was found [26]. Similar results were reported for $Rb_{0.85}(Fe_{1-y}Se)_2$, $Cs_{0.83}(Fe_{1-y}Se)_2$ and $K_{0.8}(Fe_{1-y}Se)_2$ with $I4/m$ superstructure reflections of the AFM phase present up to 12 GPa [27]. A Mössbauer study [26] also shows that the suppression of the superconductivity in $Rb_{0.8}Fe_2Se_2$ by pressure cannot be caused by a

*Corresponding author: vladimir.tsurkan@physik.uni-augsburg.de

structural transition of the minority SC phase as observed in the SC FeSe [19]. Importantly, with increasing pressure a gradual suppression of both AFM majority and SC minority phases was detected [26]. Moreover, above 5.2 GPa, the third PM phase emerges. A pronounced decrease of the hyperfine field in the AFM phase observed above 5.2 GPa points to a significant change in the local magnetic and electronic properties at the Fe sites of the majority phase [26]. A clear indication of the local structural rearrangement with pressure in SC $Rb_{1-x}Fe_{2-y}Se_2$ was provided by x-ray absorption spectroscopy which found sizable changes in the Fe *K*-edge spectra [28]. Complementary EXAFS studies performed in [28] suggested a gradual suppression of the phase separation with pressure. A lattice rearrangement to a locally more ordered state at pressures above 11 GPa was also suggested. Comprehensive high-pressure resistivity studies of insulating $Tl_{0.36}Rb_{0.44}Fe_{1.56}Se_2$, $K_{0.8}Fe_{1.6}Se_2$, and superconducting $K_{0.8}Fe_{1.7}Se_2$ and $Tl_{0.4}Rb_{0.4}Fe_{1.67}Se_2$ [29] revealed an intermediate metallic phase M‘ in both SC and non-SC samples, which develops under pressure. It was shown that the Mott insulating 245 phase coexists with the M‘ phase over a significant range of pressure up to 10 GPa, where the superconductivity vanishes. These results correlate well with those of a Mössbauer study of SC $Rb_{0.8}Fe_2Se_2$ [26], which demonstrated that the intermediate metallic phase develops with pressure at the expense of a reduction of the AFM 245 phase.

Another well-established way to probe structural and electronic correlations and to tune the critical temperature T_c of Fe-based superconductors is to induce chemical pressure via doping and substitution. For instance, the substitution of Se by Te in FeSe enhances T_c for $FeSe_{0.5}Te_{0.5}$ up to 14 K [30,31]. However, it does not allow a continuous variation of T_c by substitution. Similarly, the SC behavior in $A_{1-x}Fe_{2-y}Se_2$ systems is observed only in a narrow range of iron stoichiometry [5,18] making it difficult to unravel the correlations between structural and electronic properties. To overcome these problems Lei *et al.* [32] utilized substitution of S for Se in $K_xFe_{2-y}Se_{2-z}S_z$ which allowed to continuously tune the T_c from 33 K for $z = 0$ to a full suppression of superconductivity for $z = 1.58$. The suppression of SC state was attributed to an increasing distortion of the Fe2-Se tetrahedra and a concomitant increasing occupancy of the Fe1 sites occurring with S substitution. Here Fe1 and Fe2 refer to the two different sites of the iron ions in the crystal structure which were assumed to be nearly empty and fully occupied, respectively. It was also suggested that the increasing distortion leads to carrier localization and/or a decrease of the density of states at the Fermi energy [32].

A systematical study of substitution effect on the phase separation and superconducting behavior of $K_{0.8}Fe_{1.75}Se_{2-y}S_y$ ($0 \leqslant y \leqslant 2$) was performed in [33]. The Fe-vacancy order was reported for all samples independent on the substitution level. The T_c was found to decrease continuously from 31.2 K for $y = 0$ to 12.1 K for $y = 1.2$. The S substitution has little effect on phase separation, the two-phase microstructure with μm-size stripes being clearly distinguished even for the SC sample with the lowest T_c [33]. A new-phase separated pattern in pure sulfide $K_{0.8}Fe_{1.5+x}S_2$ with varied Fe concentration $0 \leqslant x \leqslant 0.5$ was also found [33]. Two spatially separated phases were also revealed in the semiconducting $Rb_{0.8}Fe_{1.5}S_2$ by neutron-diffraction in [34]. In addition to the block AFM (245) phase with a Néel temperature of 425 K with $\sqrt{5} \times \sqrt{5}$ Fe-vacancy order, a second phase manifesting in-plane stripe AFM order below 275 K with a rhombic Fe-vacancy order (234 phase) was detected. Further studies of $Rb_{0.8}Fe_{1.5}Se_2$ revealed two coexisting phases: a 234 AFM phase, which orders below 220 K with complex super Fe-vacancy order in addition to the rhombic Fe-vacancy order and the second AFM 245 phase with $T_N = 400$ K with a $\sqrt{5} \times \sqrt{5}$ Fe-vacancy order [35]. The phase with $T_N = 220$ K was reported earlier in [18] in samples with reduced Fe concentration. In sulfide compounds with high Fe concentration ($Rb_{0.75}Fe_{1.85}S_2$), neutron diffraction revealed two coexisting phases: a 245 phase with $T_N = 470$ K and a phase with a shorter in-plane lattice constant compared to 245 phase, which was attributed to a Fe-vacancy-free 122 phase. This phase exhibits metallic behavior as was shown by the resistivity and angle-resolved photoemission spectroscopy (ARPES) studies [36]. The neutron-diffraction studies on substituted $Rb_{0.8}Fe_2Se_{2-z}S_z$ crystals were not reported yet, however existing resistivity and ARPES data for a limited number of substitutions show that with increasing S content a gradual reduction of the SC temperature takes place, from 32 K for $z = 0$ to 9 K for $z = 1.25$. Samples with $z = 1.5$ and 2.0 manifest a metallic ground state [35,36]. The ARPES studies of $Rb_{0.8}Fe_2Se_{2-z}S_z$ with $z = 0$, 1, and 2, revealed only minimal changes in the Fermi surface topology and small changes in the charge-carrier concentration. With increasing S concentration, an increase of the overall quasiparticle bandwidth was observed indicating a decrease of electronics correlations [35]. Similar conclusion was obtained for the $K_xFe_{2-y}Se_{2-z}S_z$, $Rb_xFe_{2-y}Se_{2-z}Te_z$, and $(TlK)_xFe_{2-y}Se_{2-z}S_z$ systems in Ref. [37]. Later on, terahertz time-domain spectroscopy studies of SC and metallic $Rb_{0.75}Fe_{1.6}Se_{2-z}S_z$ on a large number of concentrations revealed a metal-to-insulator transition accompanied by an orbital-selective Mott phase transition [38,39]. It was shown that the orbital-selective Mott transition shifts to higher temperatures with increasing S concentrations indicating a reduction of correlations in the d_{xy} channel that can account for the observed suppression of T_c [38].

In the present paper, a comprehensive macroscopic characterization of single crystalline samples of $Rb_{1-x}Fe_{2-y}Se_{2-z}S_z$ studied earlier in Ref. [38] and of additional samples with narrow substitutional steps ($z = 0$; 0.1; 0.25; 0.5; 1.0; 1.1; 1.2; 1.3; 1.4; 1.7, and 2.0) is reported. The results on the stoichiometry, structure, differential scanning calorimetry, magnetic susceptibility, conductivity, and specific heat are presented. We investigate the variation of structural and electronic properties of crystals with different substitution looking for the critical concentration to suppress the SC state and for correlation effects using the advantage of the Rb-based systems to form superconducting compositions with much smaller deviations of the iron stoichiometry due to existence of robust miscibility gaps [35] compared to the related K-based system [32].

II. EXPERIMENTAL DETAILS

Single crystals of the anion-substituted $Rb_{1-x}Fe_{2-y}Se_{2-z}S_z$ have been grown by the Bridgman method. The chemical

TABLE I. Starting mixtures and real compositions of selected samples of $Rb_{1-x}Fe_{2-y}Se_{2-z}S_z$ as determined by EPMA analysis

Batch and sample label	Substitution z	Starting mixture	Concentration of the elements			
			Rb (1-x)	Fe (2-y)	Se (2-z)	S (z)
BR16	0	0.8Rb+2FeSe	0.748(27)	1.593(16)	2.000(19)	–
BR16_05	0	0.8Rb+2FeSe	0.736(40)	1.611(14)	2.000(30)	–
BR28 average	0	0.8Rb+2FeSe	0.786(39)	1.612(22)	2.000(28)	–
BR28 stripes	0		0.705(25)	2.017(10)	2.000(25)	–
BR100	0.1	0.8Rb+1.9FeSe+0.1FeS	0.750(33)	1.596(13)	1.905(22)	0.095(2)
BR99	0.25	0.8Rb+1.75FeSe+0.25FeS	0.739(26)	1.592(16)	1.752(22)	0.248(7)
BR96_le	0.5	0.8Rb+1.5FeSe+0.5FeS	0.734(25)	1.597(27)	1.511(20)	0.489(13)
BR96_1	0.5	0.8Rb+1.5FeSe+0.5FeS	0.734(24)	1.603(26)	1.507(20)	0.493(13)
BR80	1.0	0.8Rb+FeSe+FeS	0.765(23)	1.605(19)	1.017(20)	0.983(18)
BR87	1.0	0.8Rb+FeSe+FeS	0.764(27)	1.595(16)	0.998(21)	1.002(16)
BR82	1.1	0.8Rb+0.9FeSe+1.1FeS	0.844(32)	1.585(20)	0.922(23)	1.079(24)
BR107[a]	1.2	0.8Rb+0.8FeSe+1.2FeS	0.756(6)	1.600(11)	0.841(12)	1.152(12)
BR101_1	1.4	0.8Rb+0.6FeSe+1.4FeS	0.802(15)	1.620(14)	0.634(25)	1.366(16)
BR101_Ro1	1.4	0.8Rb+0.6FeSe+1.4FeS	0.791(36)	1.610(17)	0.650(23)	1.350(8)
BR102_1	1.7	0.8Rb+0.3FeSe+1.7FeS	0.822(21)	1.585(18)	0.312(16)	1.688(15)
BR97_optics	2.0	0.8Rb+2FeS	0.787(16)	1.595(11)	–	2.000(12)
BR97_1	2.0	0.8Rb+2FeS	0.735(16)	1.611(17)	–	2.000(24)

[a]Determined from the x-ray data.

composition of the samples was determined by electron-probe microanalysis (EPMA) applying wavelength dispersive x-ray spectroscopy (WDS) with a Cameca SX50 microprobe. The concentration of the elements in the studied samples was measured on freshly cleaved samples. The determined concentrations were averaged over multiple (ten to twenty) measured spots with an area of $80 \times 60\,\mu m^2$. The errors in determination of the absolute concentrations of the elements are less than 1.5% for Fe, 2% for Se and S, and 5% for Rb. The concentrations of Rb and Fe were calculated normalizing the sum of Se+S to two atoms per-formula unit.

The single crystal x-ray diffraction was performed at room temperature with an Xcalibur E diffractometer equipped with a CCD area detector and a graphite monochromator utilizing MoK_α radiation. Samples for x-ray experiments were cut from large crystal pieces and protected with Paratone-N oil. Final unit-cell dimensions were obtained and refined for the entire data set. After collection and integration, the data were corrected for Lorentz and polarization effects and for absorption by multi-scan empirical correction methods. The crystallographic structures were refined by the full matrix least-squares method based on F^2 with anisotropic displacement parameters. All calculations were carried out by the programs SHELXL2014 [40] within the package WINGX [41]. Mixed Se/S sites were refined in a similar way. In each position, the Se and S atoms were constrained to have identical coordinates and thermal parameters.

Differential scanning calorimetry (DSC) measurements were performed using a PerkinElmer DSC-8500 system. The data were collected during temperature sweeps for heating and cooling with a rate of 5 K/min. The samples were encapsulated in standard Al crucibles. During the experiments, Ar or He gases were used as protecting media. The heat flow was normalized to the mass of the samples.

Magnetic characterization was performed using a commercial SQUID magnetometer (MPMS-5, Quantum Design) for temperatures between 1.8 and 700 K, in external magnetic fields up to 5 T.The electrical resistivity and specific heat were measured with a Physical Property Measurement System (PPMS, Quantum Design) in a temperature range from 1.8 to 300 K.

III. EXPERIMENTAL RESULTS AND DISCUSSION

A. Preparation conditions and composition analysis of samples

The preparation conditions and regimes of the single crystals growth by the vertical Bridgman method were similar to those for the nonsubstituted $Rb_{1-x}Fe_{2-y}Se_{2-z}S_z$ [18]. As starting materials, polycrystalline binary compounds FeSe and FeS, preliminary synthesized from the high-purity elements: Fe (99.99%), Se(99.999%), S (99.999%), and Rb (99.75%) were used. Handling of the reaction mixtures was performed in an argon box with a residual oxygen and water content less than 1 ppm. The starting materials were placed in double quartz ampoules, pumped to 10^{-3} mbar, and then closed. The ampoules were heated to a soaking temperature of 1070 °C. The soaking time was 5 h. Then, the ampoules were pulled down in the temperature gradient of 1.5 °C/mm with a rate of 3 mm/h. The compositions of the starting mixtures for batches with different substitutions are given in Table I.

The EPMA data related to concentration of the constituent elements are also given in Table I. The EPMA analysis did not reveal any essential deviations in the S to Se ratio from the starting stoichiometry for all grown batches. The concentration of Fe in the samples from different batches was close to 1.6 indicating compositions with a Fe-vacancy corresponding to the 245 stoichiometry. We note that the deviations from the 245 stoichiometry in the $Rb_{1-x}Fe_{2-y}Se_{2-z}S_z$ system are much

TABLE IIa. Structural data and details of structural refinement for samples with substitution $z = 0$, 1, and 2 within space group $I4/m$ for $\sqrt{5} \times \sqrt{5} \times 1$ supercell.

z (nominal concentration)	0	1.0	2
x-ray composition	$Rb_{0.80}Fe_{1.61}Se_2$	$Rb_{0.76}Fe_{1.60}SSe$	$Rb_{0.78}Fe_{1.59}S_2$
Formula weight	315.65	264.95	219.58
a (Å)	8.805(1)	8.623(1)	8.462(1)
c (Å)	14.588(1)	14.352(1)	14.045(2)
Volume (Å^3)	1131.08(19)	1067.08(10)	1005.8(2)
Z/	10/	10/	10/
ρ_{calc}(gcm^{-3})	4.634	4.123	3.625
μ (mm^{-1})	29.579	22.833	15.945
Reflections	11441 / 779	8241 / 495	7574 / 520
collected / unique	$R_{int} = 0.1363$	$R_{int} = 0.0828$	$R_{int} = 0.0859$
GooF	1.005	1.002	1.004
R_1,	0.0633,	0.0458,	0.0488,
$wR_2[I > 2\sigma(I)]$	0.1946	0.147	0.1496

smaller than in $K_xFe_{2-y}Se_{2-z}S_z$ where significant variations of the Fe content from 1.44 to 1.72 on increasing substitution from $z = 0$ to $z = 2$ were reported [32].

An important observation concerns the microstructure of the studied samples. As reported earlier for nonsubstituted samples ($z = 0$) in Ref. [42], the presence of two different phases could be easily distinguished in an optical microscope with micrometer-size metallic stripes embedded into the AFM 245 phase (see Fig. 1 in Ref. [43] for microstructure of sample with $z = 0$). Under high magnification conditions, we determined the composition of these stripes, which corresponds to $Rb_{0.705(25)}Fe_{2.017(10)}Se_2$. Within experimental uncertainty, this corresponds to a Fe vacancy-free and a Rb-deficient 122 phases. This result is in general agreement with those obtained by other techniques [44,45]. A difference in Rb/Fe ratio (0.7/2) for stripes revealed by our study compared to neutron diffraction study (0.6/2.2) [44] and nuclear magnetic resonance (0.3/2) [45] can be probably attributed to difference in the accuracy of these methods.

It was further observed that for samples even with the lowest substitution $z = 0.1$, it was not possible to detect any stripe structure in the micrometer range (see Fig. 1 in Ref. [43] for microstructure of samples with $z > 0$). At the same time, the simultaneous presence of the AFM and metallic nonmagnetic

TABLE IIb. Atomic coordinates (x, y, z), site-occupation factors (sof), and thermal parameters U_{eq} (Å$^2 \times 10^3$) for Fe, Se and Rb ions within space group $I4/m$ for $\sqrt{5} \times \sqrt{5} \times 1$ supercell for samples with substitution $z = 0$, 1, and 2. U_{eq} is defined as one third of the trace of the orthogonalized U_{ij} tensor.

Z (nominal charge)			x	y	z	sof	U_{eq}
0	Atom	Position					
	Fe1	4d	0.5000	0	0.2500	0.246(13)	16(1)
	Fe2	16i	0.4069(1)	0.3015(1)	0.2480(1)	0.943(11)	19(1)
	Se1	4e	0.5000	0.5000	0.3564(1)	1	21(1)
	Se2	16i	0.2991(1)	0.1080(1)	0.3506(1)	1	22(1)
	Rb1	2b	0	0	0.5000	0.856(11)	39(1)
	Rb2	8h	0.1939(2)	0.4029(2)	0.5000	0.781(9)	37(1)
1	Fe1	4d	0.5000	0	0.2500	0.304(13)	20(1)
	Fe2	16i	0.4068(1)	0.2988(1)	0.2481(1)	0.922(14)	19(1)
	Se1	4e	0.5000	0.5000	0.3547(1)	0.496(10)	22(1)
	S1	4e	0.5000	0.5000	0.3547(1)	0.504(10)	22(1)
	Se2	16i	0.2986(1)	0.1077(1)	0.3503(1)	0.501(8)	23(1)
	S2	16i	0.2986(1)	0.1077(1)	0.3503(1)	0.499(8)	23(1)
	Rb1	2b	0	0	0.5000	0.814(10)	41(1)
	Rb2	8h	0.1953(1)	0.4044(1)	0.5000	0.742(10)	44(1)
2	Fe1	4d	0.5000	0	0.2500	0.277(10)	16(3)
	Fe2	16i	0.4073(1)	0.2967(1)	0.2479(1)	0.917(10)	16(1)
	S1	4e	0.5000	0.5000	0.3491(2)	1	19(1)
	S2	16i	0.2964(1)	0.1093(1)	0.3469(2)	1	21(1)
	Rb1	2b	0	0	0.5000	0.817(12)	35(1)
	Rb2	8h	0.1953(1)	0.4054(1)	0.5000	0.761(10)	38(1)

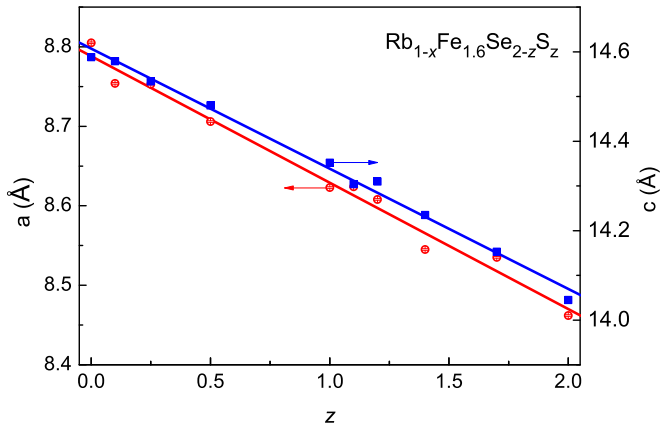

FIG. 1. Variation of the lattice parameters a and c as function of sulfur concentration z in $Rb_{1-x}Fe_{2-y}Se_{2-z}S_z$.

phases was revealed in all our $Rb_{1-x}Fe_{2-y}Se_{2-z}S_z$ samples by Mössbauer experiments [46]. This suggests that the phase separation in the anion substituted crystals in $Rb_{1-x}Fe_{2-y}Se_{2-z}S_z$ is realized on a significantly lower length scale. This is in clear contrast to $K_xFe_{1.75-y}Se_{2-z}S_z$ where the metallic stripes with micrometer size were observed even in samples with anion substitution $z = 1.2$ [33]. The difference in the microstructure of these systems can be probably attributed to a significant excess of Fe concentrations > 1.6 in K-based compared to Rb systems.

B. Structural study

The x-ray single-crystal structural analysis of the experimental pattern of $Rb_{1-x}Fe_{2-y}Se_{2-z}S_z$ reveals a tetragonal cell with lattice parameters $a(b) \sim 19$ Å, $c \sim 14$ Å for all substitutions suggesting a large $5 \times 5 \times 1$ supercell. A similar $5 \times 5 \times 1$ supercell was reported earlier by Zavalij *et al.* [47] for $K_{1-x}Fe_{2-y}Se_2$ and $Cs_{1-x}Fe_{2-y}Se_2$ crystals. Their initial structural analysis was done in a space group $I4/mmm$. However, those authors noticed the incompatibility of the space group $I4/mmm$ with the experimental data on powder neutron diffraction [5], and the structural data were further interpreted within a smaller supercell $\sqrt{5} \times \sqrt{5} \times 1$ in the space group $I4/m$ with $a(b) \sim 8.7$ Å. A similar $\sqrt{5} \times \sqrt{5} \times 1$ supercell was deduced by Pomjakushin *et al.* [48] for $Cs_yFe_{2-x}Se_2$ from the analysis of the superstructure reflections that appear below the first-order structural transformation at $T_s \sim 500$ K resulting in twinning corresponding to reflections with two propagation vectors $k_1 = [\frac{2}{5}, \frac{1}{5}, 1]$ and $k_2 = [\frac{1}{5}, \frac{2}{5}, 1]$. A similar twinning pattern was found in our $Rb_{1-x}Fe_{2-y}Se_{2-z}S_z$ samples (see Fig. 2 in Ref. [43] for reciprocal lattice plot); thus the structural refinement of all samples was performed within the generally accepted $\sqrt{5} \times \sqrt{5} \times 1$ cell, in the space group $I4/m$. The structural data and details of the structural refinement for three selected compositions (with $z = 0$, 1, and 2) are given in Tables II(a) and II(b). The full set of the structural data for all substitutions is presented in Table III in Ref. [43].

In the $\sqrt{5} \times \sqrt{5} \times 1$ supercell, all constituent elements have two different crystallographic positions (see Fig. 2 below) with different occupancies for Fe and Rb sites. The site occupancy for the Fe2 ion in a general position (x, y, z) is close to 0.93, while that of the Fe1 ion in a special position (0.5, 0, 0.25) is close to 30%. The occupancy of both Fe sites in $Rb_{1-x}Fe_{2-y}Se_{2-z}S_z$ exhibits only an insignificant change with substitution (see upper panel of Fig. 6 below). The Rb sites are also partially occupied. The occupancy of the Rb sites shows a nonmonotonous change with substitution (see Table III in Ref. [43]). It probably has to be attributed to variations of the concentration of Rb in the samples, being particularly high for

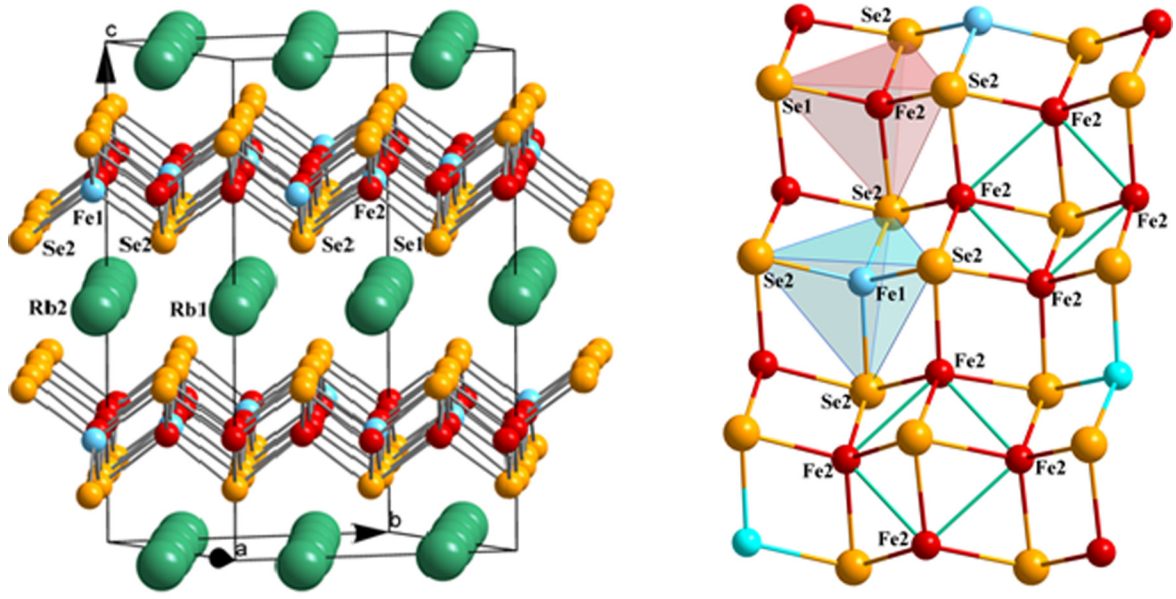

(a) (b)

FIG. 2. (a) Crystal structure of $Rb_{1-x}Fe_{2-y}Se_{2-z}S_z$ for $z = 0$. Fe1 ions are in position (0.5, 0, 0.25), Fe2 in position (x, y, z); Rb1 (0, 0, 0.5), Rb2 (x, y, 0.5), Se1(S1) in position (0.5, 0.5, z), and Se2(S2) in (x, y, z)(b) Schematic view of different Fe tetrahedrons: Fe2 with three Se2(S2) neighbors and one neighboring Se1(S1); Fe1 with four equivalent Se2(S2) neighbors. Clusters of four Fe2 ions are marked by rectangles.

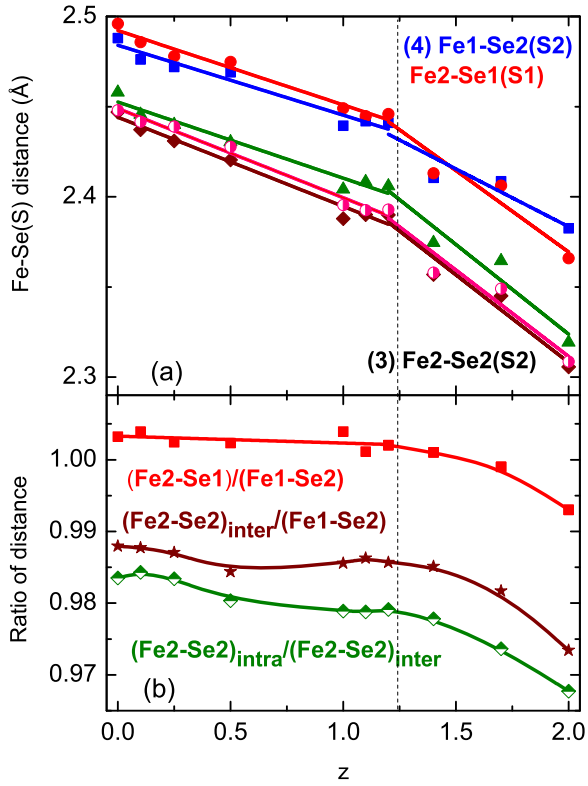

FIG. 3. Structural variations with sulfur concentration z. Frame (a): four equivalent Fe1-Ch2 bond distances, Fe2-Ch1 bond distance and three Fe2-Ch2bond distances. Frame (b): ratio of Fe2-Ch1 bond distance to Fe1-Ch2, intercluster Fe2-Ch2 distances to Fe1-Ch2, intracluster Fe2-Ch2 distances to intercluster Fe2-Ch2. Vertical dashed line separates superconducting samples from nonsuperconducting ones.

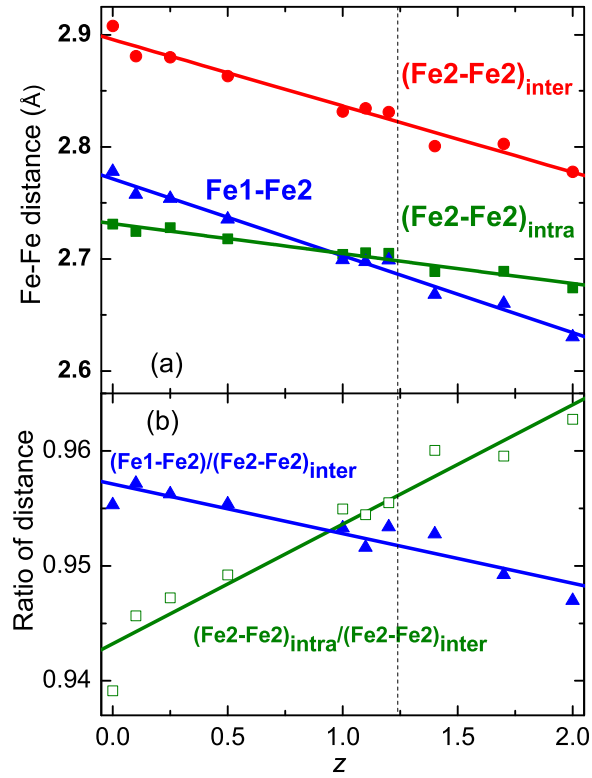

FIG. 4. Structural variations with sulfur concentration z. (a) Intercluster Fe2-Fe2 distances, intracluster Fe2-Fe2 distances, and Fe1-Fe2 distances. (b) Ratio of Fe1-Fe2 to intercluster Fe2-Fe2 distance, intracluster Fe2-Fe2 to intercluster Fe2-Fe2 distance.

samples with substitution $z = 1.1$ (see Table I). The reason of these variations of Rb concentration is unclear at the moment and needs additional studies.

In Fig. 1, the variations of the lattice parameters a and c with substitution are presented. Both parameters show a close to linear decrease with increasing sulfur content following Vegard's law indicating the formation of continuous solid solutions in this system due to substitution of S for Se. This fact together with the absence of any additional changes in the lattice symmetry with substitution indicates statistical substitution of Se by the S ions in the anion positions.

The local tetrahedral environment of Fe2 ion consists of three nearly equivalent Fe2-Se2(S2) bonds and one Fe2-Se1(S1) bond, while the local environment of Fe1 ion consists of four equivalent Fe1-Se2(S2) bonds as shown in Fig. 2(b). Four Fe2 ions form clusters with shorter intracluster and larger intercluster distances Fe2-Fe2.

To get insight into the local distortions of the Fe1 and Fe2 tetrahedrons and their evolution with substitution, we analyzed the bond distances between the Fe ions, between the Fe ions and chalcogens (Ch = Se or S), as well as their bond angles. A monotonous close to linear decrease with the substitution of the bond distances Fe-Ch for both tetrahedrons was found for $z \leqslant 1.2$ (see Fig. 3(a) and Table IV in Ref. [43]), as anticipated for the observed decrease of the unit cell parameters a and c with substitution (Fig. 1). We also noticed that the rate of the decrease of all Fe-Ch distances is notably higher for substitution $z > 1.2$ than for $z \leqslant 1.1$. Particularly, this behavior is more pronounced for the Fe2-Se(S)2 bond distances. It must be noted that in the substitution range $1.1 \leqslant z \leqslant 1.4$ a slightly increased concentration of Rb compared to other substitutions was observed. Therefore, for this substitution range to account for variation of the Fe-Ch bond distances two variables, x and z, should be considered. At the same time, within the observed range of variation of the Rb concentration in the studied system (0.74–0.84) we did not found a clear correlation between the lattice parameters and the Rb concentration (see Fig. 2 in Ref. [43]). Furthermore, the lattice parameter c for sample with substitution $z = 1.1$ and the highest Rb concentration 0.84 was very close to that of the sample with $z = 1.2$ and significantly lower Rb concentration 0.76. The rate of change of the anion height with z [Fig. 6(b)] that is directly related to distances Fe-Ch was also notably higher for samples with substitutions above 1.2 compared to those for z below 1.2. Therefore, within the observed range, we conclude that the variation of the Rb concentration cannot essentially contribute to the change of the bond distances Fe-Ch. In addition, we observed that for the substitution range $z \leqslant 1.2$, the ratio of the Fe2-Ch2 bond distances to the Fe1-Ch2 distance changes slightly, whereas above $z = 1.2$, it decreases essentially [Fig. 3(b)]. This also suggests a small influence of the difference in the Rb concentrations on the variation with substitution of the Fe-Ch bond distances for both Fe1 and Fe2 tetrahedrons. As

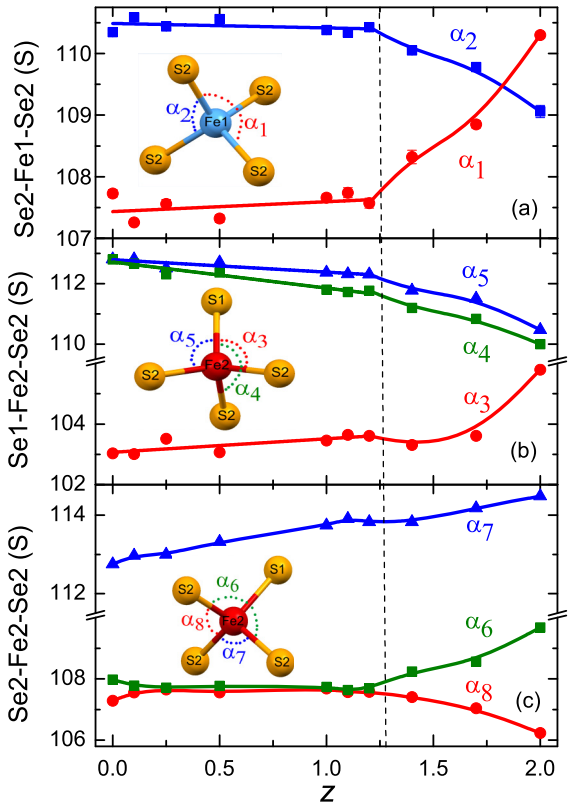

FIG. 5. Variation with substitution of bond angles (in degrees). (a) Fe1 tetrahedron (two angles α_1 and four angles α_2. [(b) and (c)] Fe2 tetrahedron (angles from α_3 to α_8). Vertical dashed line separates superconducting samples from the nonsuperconducting ones.

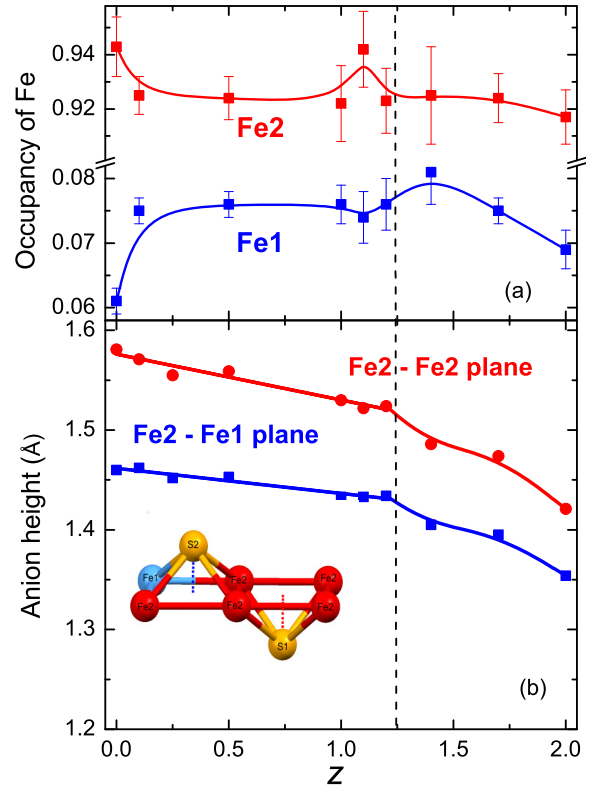

FIG. 6. Variations with substitution: of occupancy of Fe1 and Fe sites (a), and of anion-height from Ch (Se,S) to Fe2-Fe1 plane and from Ch to Fe2-Fe2 plane (b).

will be shown below, the superconductivity in the samples vanishes just above $z = 1.2$. It should be mentioned that the observed behavior of the bond distances Fe-Ch with substitution is very similar to that reported for Fe-Se distances in SC $Rb_{1-x}Fe_{2-y}Se_2$ under external pressure. The Fe-Se distances show gradual (linear) decrease with pressure manifesting a steplike drop in the range where the SC state becomes fully suppressed [28].

We also found that the Fe1-Fe2 distance and the intercluster Fe2-Fe2 distance show a much stronger decrease with the substitution than the intracluster Fe2-Fe2 distance [Fig. 4(a)]. The observed variations of the Fe-Fe distances with substitution are in good agreement with those reported for $K_xFe_{2-y}Se_{2-z}S_z$ [32]. It should be noted that the ratios of the Fe1-Fe2 distance to the intercluster Fe2-Fe2 distance and that of the intracluster Fe2-Fe2 distance to the intercluster Fe2-Fe2 distance exhibit an opposite trend with substitution [Fig. 4(b)] intercepting in the range close to $z = 1.2$. It is also worth mentioning that, with increasing substitution, the ratio of the intracluster to intercluster Fe2-Fe2 distances increases and approaches unity suggesting a more regular in-plane structural arrangement.

In Figs. 5(a)–5(c), the variations of the bond angles for Fe1 and Fe2 tetrahedrons with substitution are presented. In the Fe1 tetrahedron, four large angles α_1 and two small angles α_2 exhibit a tendency to approach the ideal angle of 109°47′ on increasing concentration up to $z = 2.0$ [see Fig. 5(a)]. A similar trend is found for the other four angles α_3, α_4, $\alpha 5$ and α_6 in the Fe2 tetrahedron, while the remaining two angles α_7 and α_8 of this tetrahedron increase and, respectively, decrease with substitution [see Fig. 5(c)]. An analysis of the regularity of Fe tetrahedrons by comparing the sum of the angles at the Ch1 and Ch2 vertices has shown that with increasing substitution from $z = 0$ to $z = 2$, the Fe2 tetrahedron becomes more regular indicating decreasing distortions. This fact is in a clear contrast to that reported for $K_xFe_{2-y}Se_{2-z}S_z$ system, where increasing distortions with increasing S concentration were observed and were suggested to destroy the SC state [32].

Looking for a possible optimization of the structural parameters, we have analyzed the variations of the anion height with substitution. Both anion heights of the Ch1 to the Fe2 plane and of the Ch2 to the Fe1-Fe2 plane were found to exhibit a continuous decrease with concentration as shown on the lower panel of Fig. 6. This behavior is also in a strong contrast to that observed in $K_xFe_{2-y}Se_{2-z}S_z$ that shows a nonmonotonic behavior with substitution [32].

C. Differential scanning calorimetry

Figures 7(a)–7(d) show the DSC results for several selected $Rb_{1-x}Fe_{2-y}Se_{2-z}S_z$ crystals with different sulfur concentration z. The full set of the DSC data for the studied crystals is given Figs. 4(a)–4(h) in Ref. [43]. The DSC signal corresponds to a difference in heat required to increase the sample temperature with respect to the reference (empty Al crucible).

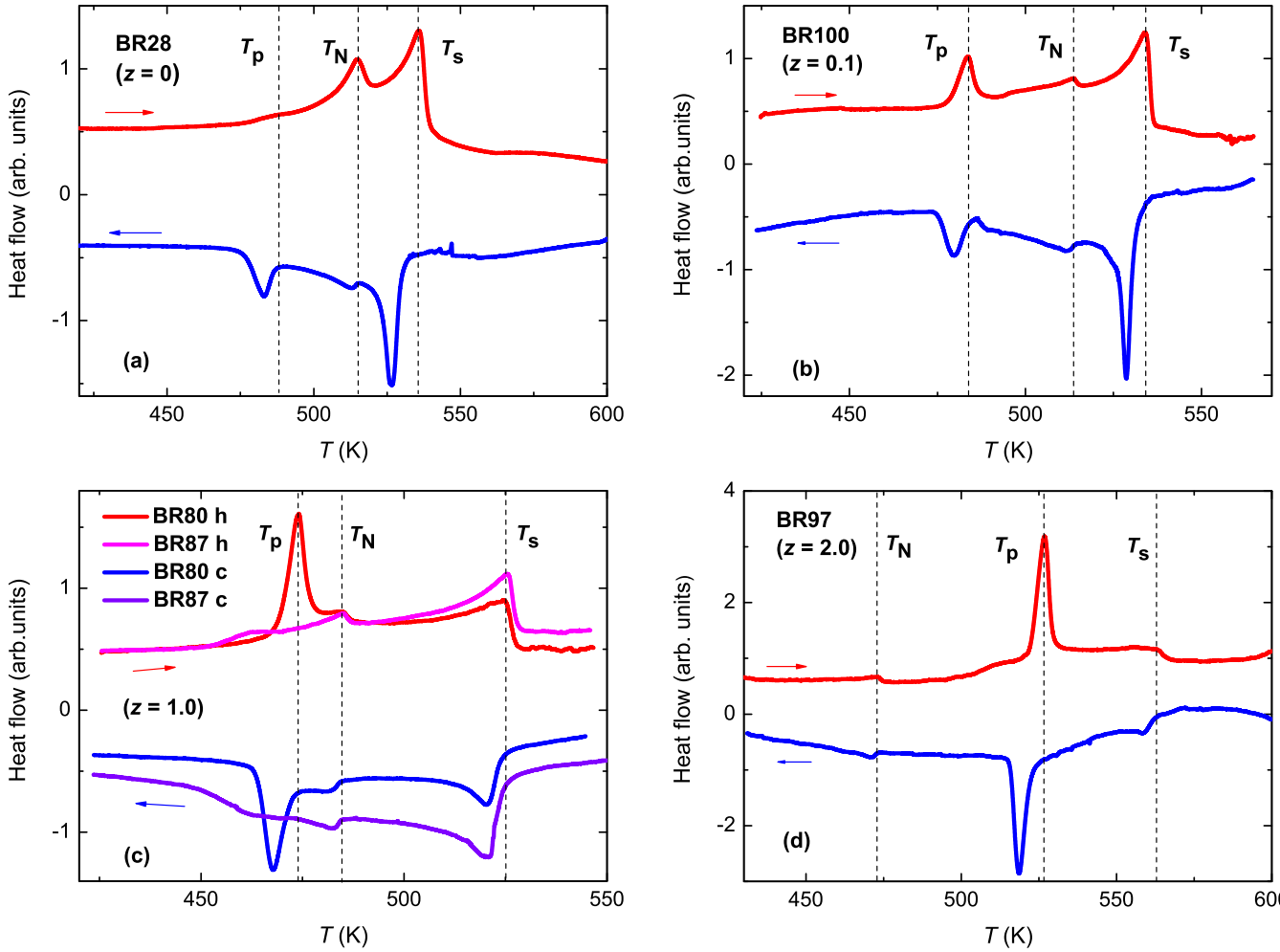

FIG. 7. Temperature dependence of DSC signals for $Rb_{1-x}Fe_{2-y}Se_{2-z}S_z$ crystals with different sulfur concentration z: (a) $z = 0$, (b) 0.1, (c) 1, and (d) 2. Red curves show data on heating, blue ones on cooling. Vertical dashed lines mark phase transition temperatures on heating.

For the nonsubstituted sample [Fig. 7(a), $z = 0$] on increasing temperatures from 300 to 600 K, three clear anomalies were recorded. The temperature positions of these anomalies were very close to those found for the as-grown $Rb_xFe_{2-y}Se_2$ single crystals studied by the DSC technique in Refs. [44,49]. The neutron diffraction studies, also performed in Ref. [44], allowed assigning the anomaly in the DSC signal at the highest temperature T_s to a structural transition of the majority 245 phase from the vacancy-disordered state into the state with ordering of Fe vacancies. The anomaly at T_N at intermediate temperature was assigned to a transition of the 245 phase into the AFM state. The anomaly at the lowest temperature at T_p was attributed to a phase-separation temperature, where the Rb-deficient 122 phase segregates from the 245 phase [44].

Inspection of the observed anomalies in the DSC signal for our $Rb_{1-x}Fe_{2-y}Se_{2-z}S_z$ crystals reveals that the anomalies at T_s and T_p exhibit significant hysteresis (up to 10 K) on cooling and heating cycles indicating that they are related to the first-order structural transformations. The anomaly at T_N shows the smallest hysteresis (2 K) as expected for a second-order magnetic transformation.

The structural anomaly at T_p shows complex behavior. In samples with substitution $z \leqslant 1.0$ this anomaly was discernible in the DSC signal as a small step or distinct maximum on heating [see Figs. 7(a) and 7(b)]. In the samples with the steplike anomaly at T_p it was evidenced as well-defined minimum better seen on cooling. Even for samples from different batches but with the same concentration $z = 1.0$, the anomaly at T_p showed a completely different appearance on heating, although the other two anomalies at T_N and T_s were quite similar both for heating and cooling cycles [see Fig. 7(c)]. We found no difference in the magnetic behavior of these samples in the non-SC state. In the SC state they show a notable difference in the low-field range (see Fig. 5 in Ref. [43]) and a significant difference in their resistivity behavior. The sample with a higher height of the anomaly at T_p in the DSC signal shows a much lower value of the residual resistivity (see Fig. 6 in Ref. [43]). The transition at T_m from metallic to semiconductor-like behavior of the resistivity for this sample is shifted to higher temperatures compared to that for the sample with smaller height of the anomaly at T_p. Such a difference in the resistivity behavior can be related either to different amount of the minority (SC) phase or different distribution of the minority phase network in these samples. It is necessary to mention that heat-treatment experiments on $Rb_xFe_{2-y}Se_2$ superconductors demonstrated that the

distribution of the minority metallic phase in samples can be changed significantly by annealing, yielding a similar reduction of the resistivity and shift of T_m to higher temperatures, but not affecting the volume fractions of the majority AFM and minority metallic phases [49]. Therefore, the difference in the resistivity behavior and in the height of the anomaly at T_p in the DSC as well as the difference in low-field magnetic behavior in the SC state for samples with $z = 1.0$ can be mostly related to different distributions of the SC phase in the bulk of these samples. In addition, a considerable increase of the height of the anomaly at T_p for the nonsubstituted sample observed on the cooling cycle compared to the heating curve [Fig. 7(a)] can be also interpreted as due to a change in the distribution of the minority phase by annealing even during such a short time. Thus, from annealing experiments reported in literature and our data, we conclude that the appearance of the anomaly at T_p depends on the distribution of the minority phase in the bulk that can be affected by details of cooling process during the crystal growth or during the DSC measurements.

For the intermediate range of substitution $1.1 < z < 1.3$, the anomaly at T_p was hardly detectable (see Fig. 4(e) in Ref. [43]). Since in this substitution range the superconductivity vanishes, one would intuitively associate this behavior with a reduction of the amount of the minority SC phase. It should be noted here that the suppression of the phase separation was suggested to take place at the threshold of suppression of the SC state observed in the pressure experiments [28]. However, from the Mössbauer experiments we know that two different phases are always present in the samples independent of substitution [46]. Therefore, the absence of an anomaly at T_p does not necessarily signals that the phase separation vanishes. Moreover, for samples with concentration $z \geqslant 1.3$, the height of the anomaly at T_p in the DSC signal becomes large again, being even larger than the height of the anomalies at T_N and T_s(see Fig. 7(d) and Figs. 4(f)–4(h) in Ref. [43]). The observed strong hysteresis on heating and cooling still allows associating this anomaly with the structural transformation. However, the highly enhanced enthalpies of the transition at T_p compared to those of the other two anomalies at T_N and T_s suggests a different origin of the metallic phase that is present in samples with high S substitution. A modification of the distribution of the minority phase resulting in microstructural changes that takes place in samples in the substitutional range $1.1 < z < 1.3$ can also not be excluded. The significant difference in the magnetic and conducting properties of SC samples with $z = 1.1$ and 1.2 compared to SC sample with $z = 1.0$ (discussed in the following sections) may reflect these microstructural changes.

It was further observed that, while the anomaly at T_s is well separated from the anomalies at T_p and T_N for the whole range of substitution, the values of T_p and T_N in the range $1.1 < z < 1.4$ become close to each other. These merging effects make it difficult to distinguish the anomaly at T_N due to its lower intensity in the DSC curve compared to that of the anomaly at T_p. Therefore, to have an additional proof of the origin of the anomalies at T_N and T_p, susceptibility studies of our samples in the temperature range 300–600 K were carried out. The respective data are given in Figs. 7(a)–7(e) in Ref. [43]. All three anomalies revealed in the DSC measurements were distinguishable and identified as clear steps or change of slope in the susceptibility or inverse susceptibility data. A good agreement of the phase-transition temperatures T_s, T_p, and T_N was observed in DSC and magnetic-susceptibility. A comparison of the hysteretic behavior of these anomalies allowed getting reliable assignment of the structural and magnetic transformations.

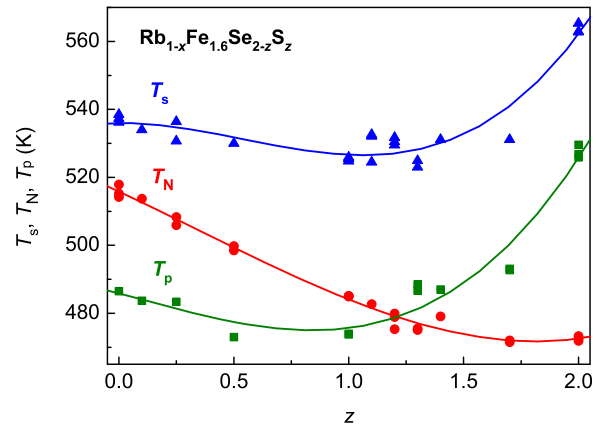

FIG. 8. Concentration dependence of the structural phase transition temperatures T_s, and T_p, and of the magnetic transformation T_N for $Rb_{1-x}Fe_{2-y}Se_{2-z}S_z$. Data are taken from DSC curves measured on heating. Solid lines are drawn to guide the eye.

Figure 8 shows the variations of the temperatures of the structural and magnetic transformations with substitution as derived from the DSC data on heating. The structural transitions exhibit a nonmonotonic change with substitution with a small decrease of T_s and T_p in a range of $0 < z < 1.2$ followed by a strong increase of their values for $z > 1.3$. At the same time, T_N changes monotonously decreasing from 515 K (for $z = 0$) to 472 K (for $z = 2$) indicating strong decrease of the AFM interactions with increasing sulfur concentration z. Note that the value of T_N for the pure sulfide sample ($z = 2$) is very close to $T_N = 470$ K determined from the neutron-diffraction measurements for a crystal with nominal composition $Rb_{0.8}Fe_2S_2$ [35] supporting our results.

D. Magnetic susceptibility and hysteresis

Figures 9(a) and 9(b), respectively, present the temperature dependencies of the magnetic susceptibility, $\chi_{||}$, for superconducting and nonsuperconducting samples with different substitutions measured in a magnetic field $H = 10$ kOe applied parallel to the c axis. For the substituted samples, $\chi_{||}$ shows a nonlinear increase with temperature similar to pure $Rb_{0.8}Fe_{1.6}Se_2$ [18]. With increasing concentration z up to 1.2, the susceptibility exhibits an insignificant increase in the value just above the SC transition. For the nonsuperconducting samples with $z \geqslant 1.3$, the susceptibility shows very similar over-all temperature dependence as for samples with $z \leqslant 1.2$ above the SC transition. In addition, in Fig. 9(b), the susceptibility $\chi_\perp$ versus temperature is shown for the sample with $z = 2$ measured in a configuration with the magnetic field applied perpendicular to the c axis. Except for the temperatures below 50 K, the susceptibility $\chi_\perp$ is significantly enhanced and shows very little change with temperatures. A

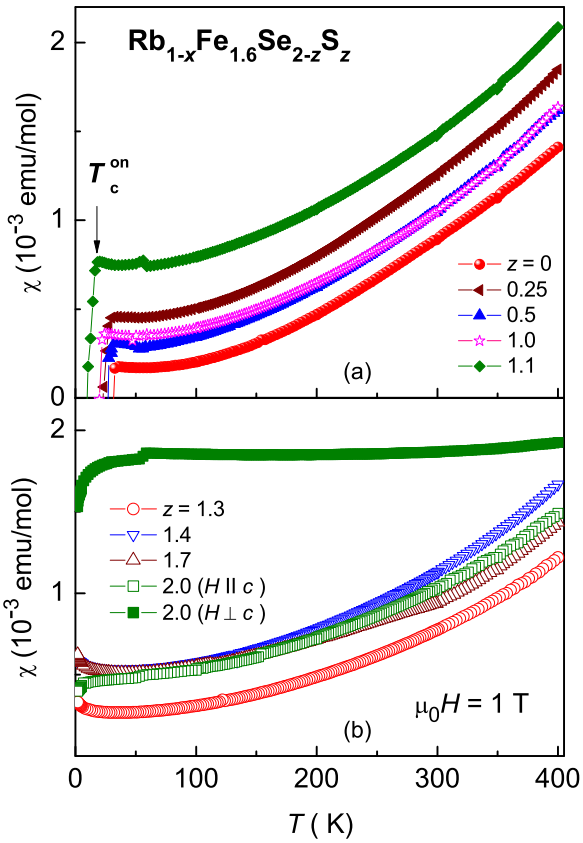

FIG. 9. Temperature dependent susceptibility $\chi_{||}$ for superconducting (a) and nonsuperconducting (b) $Rb_{1-x}Fe_{2-y}Se_{2-z}S_z$ samples measured in an external magnetic field of 1 T applied along c axis. Arrow indicates the SC transition temperature for the sample with $z = 1.1$. Additionally, the susceptibility $\chi_{\perp}$ measured in a magnetic field applied perpendicular to the c axis is shown for the sample with $z = 2$.

similar behavior of the temperature-dependent susceptibility $\chi_{\perp}$ with temperature was found for all samples studied in the course of these experiments. The observed behavior of $\chi_{\perp}$ and $\chi_{||}$ is characteristic for an antiferromagnet with the spins aligned along the c axis and is a distinct feature for the whole $Rb_{1-x}Fe_{2-y}Se_{2-z}S_z$ system.

Figure 10 presents the temperature dependent zero-field cooled (ZFC), χ_{ZFC}, and field-cooled (FC), χ_{FC}, susceptibilities for superconducting samples with different substitutions measured in a field $H = 10$ Oe applied parallel to the c axis. The value of the FC susceptibility (Meissner effect) is small due to strong pinning effects. At the same time, the value of the ZFC susceptibility indicates a 100% shielding effect for the samples with z up to 1.2, although the volume fraction of the SC phase is small. With increasing substitution from 0 to 1.2, a continuous reduction of the superconducting transition temperature from 32.4 to 10 K is observed, however, with a nonmonotonous change at the substitution level of 1/8. This sample with $z = 0.25$ shows a lower transition temperature T_c of 25 K than the sample with the higher concentration $z = 0.5$ with $T_c = 28$ K. The transition into the SC state for the samples with the substitution up to $z = 1.0$ is rather sharp. No broadening of the SC transition width for this

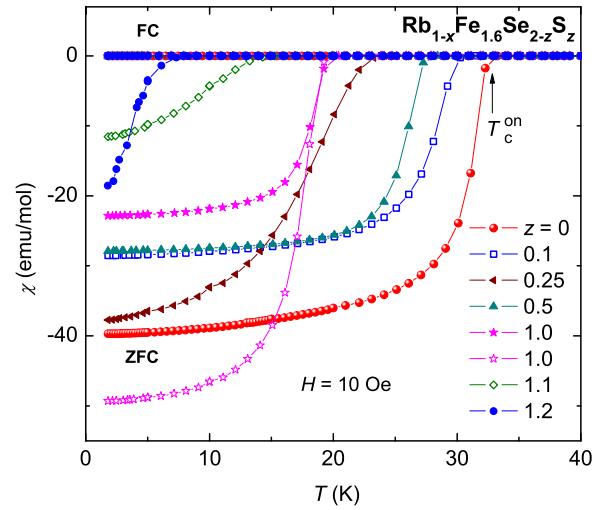

FIG. 10. Temperature dependent susceptibilities (ZFC and FC) for different superconducting $Rb_{1-x}Fe_{2-y}Se_{2-z}S_z$ samples measured in an external magnetic field of 10 Oe applied along c axis. Arrow indicates the temperature of the onset of superconducting transition for the sample with $z = 0$.

substitution range was observed compared to nonsubstituted samples (again with exception of the sample with $z = 0.25$). The sample with $z = 1.2$ exhibits the lowest SC transition temperature close to 10 K. Thus our magnetic studies revealed that the threshold for the appearance of superconductivity in $Rb_{1-x}Fe_{2-y}Se_{2-z}S_z$ crystals is placed between $z = 1.2$ and 1.3. It differs essentially from the $K_xFe_{2-y}Se_{2-z}S_z$ system where the SC state was reported up to a substitution $z = 1.6$ [32].

Figure 11 presents magnetization hysteresis loop (MHL) for SC samples with different substitution measured at 2 K with the magnetic field H applied along the c axis. The MHL for nonsubstituted sample exhibits a minimum in magnetization near zero field. Similar feature was observed by

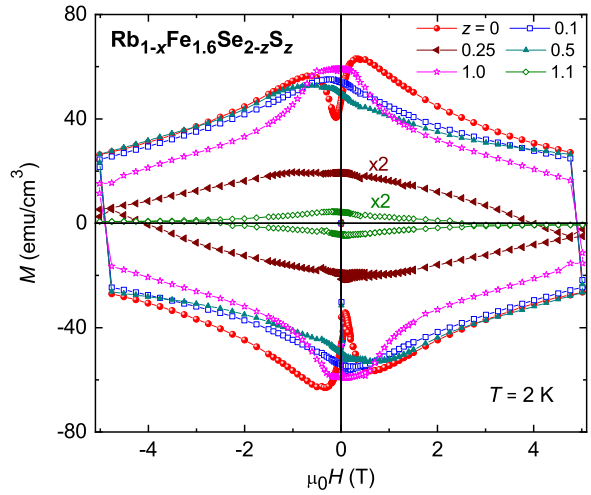

FIG. 11. Hysteresis loops measured at 2 K with the magnetic field applied along c axis for different superconducting $Rb_{1-x}Fe_{2-y}Se_{2-z}S_z$ samples.

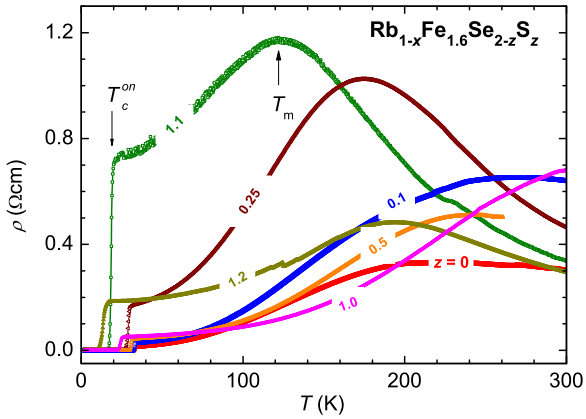

FIG. 12. Temperature dependence of the electrical resistivity for superconducting $Rb_{1-x}Fe_{2-y}Se_{2-z}S_z$ with concentrations as indicated in the figure. Arrows indicate critical temperatures.

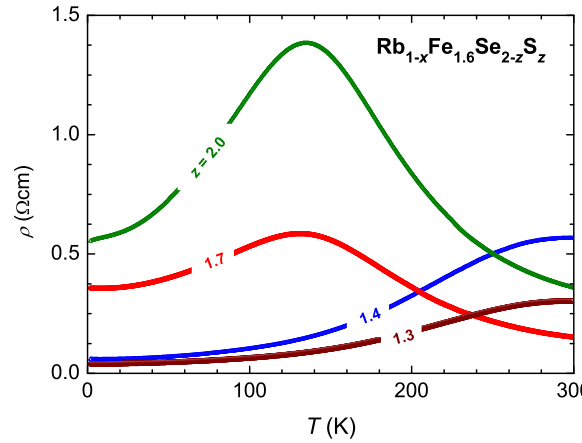

FIG. 13. Temperature dependent resistivity for nonsuperconducting $Rb_{1-x}Fe_{2-y}Se_{2-z}S_z$ for sulfur concentrations z as indicated in the figure.

Shen *et al.* [50] in the MHL of superconducting $K_xFe_{2-y}Se_2$ crystals. It was attributed to a two-step penetration of magnetic field in the bulk of the samples. The minimum in the magnetization near zero field was interpreted in terms of a phase-separation scenario of percolating superconductivity of weakly coupled superconducting islands embedded within a nonsuperconducting matrix.

The diamagnetic response (i.e. the area of the loop) of the samples with the substitution range up to $z = 1.0$ (except for the sample with $z = 0.25$) is very similar to that of the nonsubstituted sample ($z = 0$). However, compared to the sample with $z = 0$, no minimum in magnetization near zero field is observable in the MHL for the substituted samples, even for a minor concentration $z = 0.1$. This fact suggests a significant change of the flux profile that occurs as a function of concentration, which can be attributed to a difference in the distribution of the SC phase in these samples. As already mentioned, changes of the spatial distribution of the SC phase can be concluded from changes of the microstructure (see Fig. 1 in Ref. [43]). A lower diamagnetic response observed for sample with $z = 1.1$ may result from z approaching the critical range of suppression of the SC state in this system, and concomitantly from the reduction of the amount of SC phase. The reason for the strong reduction of the diamagnetic response for the sample with $z = 0.25$ is unclear and this anomalous behavior deserves further studies.

E. Resistivity

Figures 12 and 13 show the temperature-dependent resistivity of superconducting and nonsuperconducting samples, respectively. The resistivity for both types of samples exhibits nonmonotonic temperature dependence with semiconductor-like behavior at high temperatures, a broad maximum at T_m on decreasing temperature followed by a metallic-like behavior below T_m. In the $Rb_{1-x}Fe_{2-y}Se_{2-z}S_z$ system, the temperature T_m was found to show a nonmonotonic variation with substitution. In fact, the observed temperature dependence of the resistivity of our samples is typical for the whole family of $A_{1-x}Fe_{2-y}Se_2$ superconductors. Shoemaker *et al.* described such a nonmonotonic temperature behavior of the resistivity observed in the SC $K_{0.85}Fe_{1.9}Se_2$ sample by two percolating phases: one, minority phase, with metallic, and the other, majority phase, with insulating behavior [51]. The change of the temperature position of the maximum of the resistivity at T_m was attributed to a variation of the relative volume fraction of these two phases. For superconducting crystals with substitution $z \leqslant 1.2$ we have registered a lower value of T_m for samples with a higher residual resistivity in the normal state. This, however, cannot be exclusively attributed to a decrease of the volume fraction of the metallic (SC) phase. Indeed, as was discussed in Section C, the significant difference (by a factor of five!) in the residual resistivity in the normal state and in the values of T_m for two SC samples with the same concentration $z = 1.0$ and similar volume fraction of the majority insulating phase (see Fig. 6 in Ref. [43]), points to a significant influence of the distribution of the minority metallic phase on the resistivity behavior of the samples. Although the residual resistivity in the normal state for samples with substitution $z \leqslant 1.2$ shows a general trend of increasing values with increasing sulfur content (see Fig. 8 in Ref. [43]), several exceptions, e.g., the resistivity behavior of samples with $z = 0.25$ and 1.1 still need to be clarified, requiring additional studies.

Figure 14 demonstrates the temperature dependent resistivity measured in different magnetic fields applied in the vicinity of the superconducting transition for $Rb_{1-x}Fe_{2-y}Se_{2-z}S_z$ with substitution $z = 0.1$, 0.25, 1.0, and 1.2. The data for other substitutions are given in Fig. 9 in Ref. [43]. In zero field, the transition temperature of the substituted samples determined at the level of a 90% drop of the normal-state resistivity differs by 1 to 2 K from that of the onset temperature T_c estimated from the susceptibility measurements. In pure $Rb_{0.8}Fe_{1.6}Se_2$, this difference does not exceed 0.1 K [18]. This suggests an increasing inhomogeneity of the samples which can be probably attributed to substitutional disorder. When increasing the magnetic field, the resistivity curves are shifted to lower temperatures. Figure 15 shows the temperature dependence of the upper critical field $H_{c2}(T)$ for samples with different substitution level estimated by using the criterion of a 90% drop of the normal-state resistivity. The estimation of the

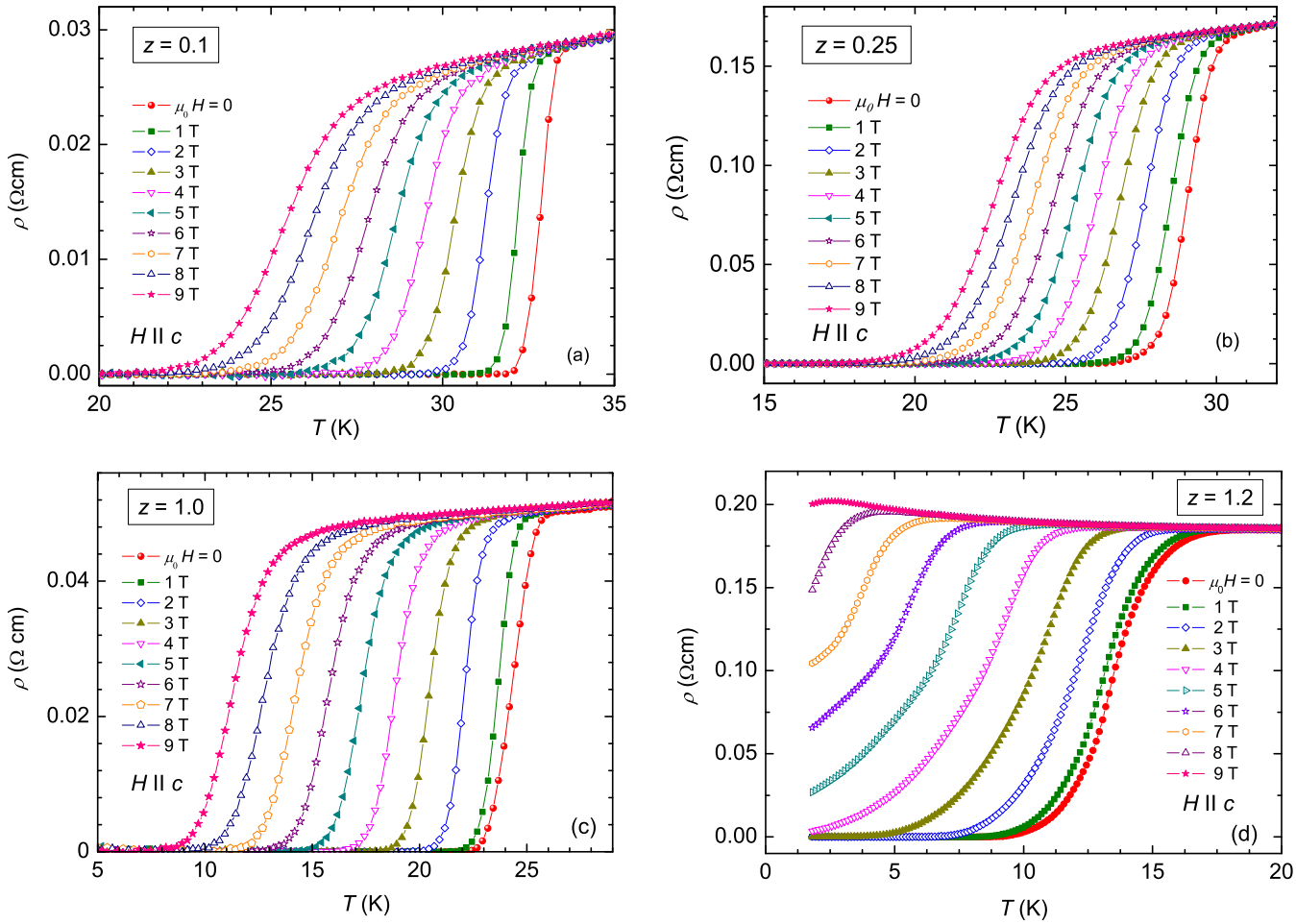

FIG. 14. Temperature dependent electrical resistivity in different applied magnetic fields in the vicinity of superconducting transition for $Rb_{1-x}Fe_{2-y}Se_{2-z}S_z$ with sulfur concentrations: (a) $z = 0.1$, (b) 0.25, (c) 1.0, and (d) 1.2.

upper critical field $H_{c2}(0)$ for $T = 0$ K was performed with the Werthamer-Helfand-Hohenberg model [52] using the relation $H_{c2}(0) = -0.69T_c(dH_{c2}(T)/dT)|_{Tc}$. The upper critical field increases from 22 T for $z = 0$ to 35 T with increasing sulfur substitution up to $z = 0.25$, but then decreases with a further growth of the sulfur content in the samples, going down to the value of 9 T for $z = 1.1$ (as shown in Fig. 16). It is noteworthy that the sample with $z = 0.25$ with a smaller T_c compared to the pure selenide compound (with $z = 0$) shows the highest value of the upper critical field.

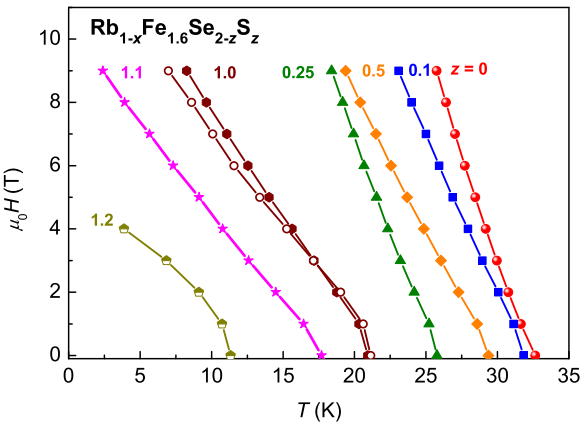

FIG. 15. Temperature dependence of upper critical field H_{c2} for samples with different sulfur concentrations as indicated in the figure.

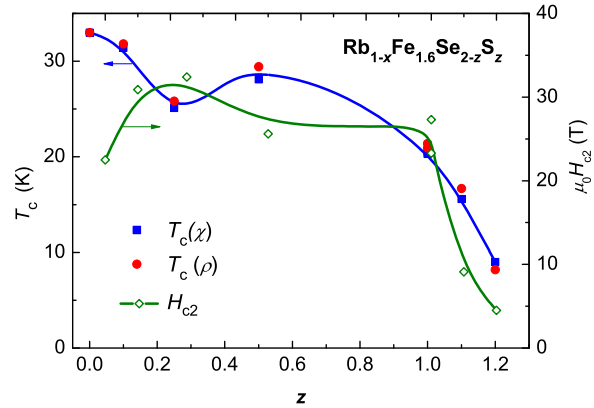

FIG. 16. Concentration dependence of the critical temperature T_c (left scale) and of upper critical field $H_{c2}(0)$ (right scale). Closed circles and squares show T_c estimated from resistivity and susceptibility measurements, respectively. Lines are drawn to guide the eye.

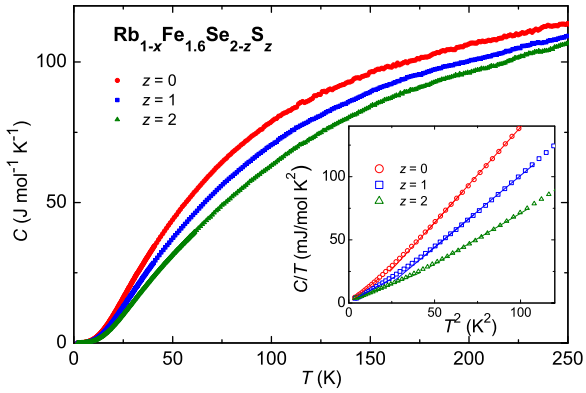

FIG. 17. Temperature dependent specific heat C for selected $Rb_{1-x}Fe_{2-y}Se_{2-z}S_z$ samples with different sulfur concentrations as indicated in the figure. The inset shows C/T vs T^2 . The solid lines represent fits as described in the text.

F. Specific heat

Figure 17 presents the temperature-dependent specific heat C for selected samples with different sulfur concentrations. In the measured temperature range, the specific heat for both superconducting and nonsuperconducting samples exhibits quite similar behavior being dominated by the lattice contribution. For the superconducting samples, the anomaly at the critical temperature is hardly detectable in the raw data. However, these anomalies become clearly visible after subtraction of lattice and magnetic contributions from the total specific heat C. The data for the electronic specific heat $C_{\rm el}$ of several nonsubstituted samples $Rb_{0.8}Fe_{1.6}Se_2$, are shown in Fig. 18.

An important problem for the calculation of $C_{\rm el}$ is related to the determination of the phonon, $C_{\rm lat}$, and magnetic, $C_{\rm m}$, contributions. In Ref. [18], it was shown that an insulating sample $Rb_{0.75}Fe_{1.5}Se_2$ exhibits very similar magnetic properties like superconducting $Rb_{0.8}Fe_{1.6}Se_2$. The present study of $Rb_{1-x}Fe_{2-y}Se_{2-z}S_z$ system also revealed quite similar antiferromagnetic behavior of all samples independent of substitution. Therefore, for modelling the phonon and magnetic contributions, the specific-heat data for the nonsuperconducting samples $Rb_{0.75}Fe_{1.5}Se_2$ with $C_{\rm lat}(0)$ for $z = 0$, and $Rb_{0.8}Fe_{1.6}S_2$ with $C_{\rm lat}(2)$ for $z = 2$ were used. For the substituted samples, this contribution was calculated taking into account the respective weight of $C_{\rm lat}(0)$ and $C_{\rm lat}(2)$, e.g., $0.5[C_{\rm lat}(0) + C_{\rm lat}(2)]$ for $C_{\rm lat}(1)$, $0.5[C_{\rm lat}(0) + C_{\rm lat}(1)]$ for $C_{\rm lat}(0.5)$], *etc*.

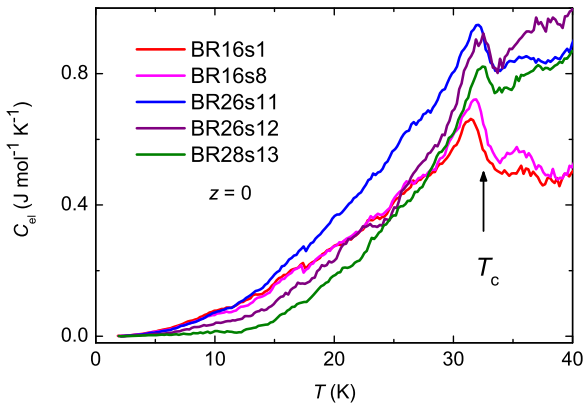

FIG. 18. Temperature dependent electronic specific heat $C_{\rm el}$ for $Rb_{0.8}Fe_{1.6}Se_2$ samples ($z = 0$) from different batches. Arrow marks T_c taken from the susceptibility data.

The inset in Fig. 17 shows the temperature dependent specific heat in the representation C/T versus T^2 at temperatures below 10 K for samples with $z = 0$, 1, and 2. These dependencies display two linear regimes: one below 4.5 K and the other in the temperature range from 7 to 10 K. Assuming that in the lower linear regime the superconducting contribution to heat capacity is much smaller than in the second one, the experimental data at temperatures below 4 K were fitted by the expression $C/T = \gamma_0 + \beta T^2$. Here γ_0 is the coefficient for the term in the specific heat that is linear in temperature and the prefactor β characterizes the lattice and magnon contributions to the specific heat, which are both proportional to T^3 and cannot be estimated independently because the AFM transition temperature T_N and the Debye temperature θ_D are comparable. The calculated values of the parameters γ_0 and β are given in Table III. The phonon and magnetic contributions for the superconducting samples with substitutions $z \leqslant 1.2$ were corrected for the difference in their effective Debye temperatures, when comparing with the value θ_D for the modelled nonsuperconducting contribution [53]. The effective Debye temperature was calculated from the relation $\theta_D = [12\pi^4 k_B N_A Z/(5\beta)]^{1/3}$, where $k_{\rm B}$ and $N_{\rm A}$ are the Boltzmann and the Avogadro constants, respectively. Z = 5, is the number of atoms in the unit cell. The calculated values of θ_D for all studied samples are also presented in Table III.

The determined values of γ_0 were found to vary in a range 0.08-0.3 mJ/(mol K^2) for all samples with substitution $z \leqslant 1.1$ (with exception of sample with $z = 0.25$). Even for a given z, the spread of experimental values of γ_0 is rather large indicating variations of the growth-dependent pair-breaking mechanisms. The reason for this variation is probably originating from the phase-separated nature of the system. Besides the pair-breaking effects of substitutional disorder and residual impurities occurring in single-phase superconductors, the proximity to the AFM phase and the orbital-selective contribution of the charge carriers in the normal and superconducting phases will be sources of pair breaking which vary both with the substitution z and with temperature and, therefore, cannot easily be estimated quantitatively.

We note also that a value of $\gamma_0 = 0.394$ mJ mol^{-1}K^{-2} was reported for a superconducting sample $K_xFe_{2-y}Se_2$ in Ref. [54]. For our samples with $z \geqslant 1.2$, the value of γ_0 increased significantly suggesting an increasing amount of metallic phase.

The value of the prefactor β shows a continuous decrease with increasing substitution in agreement with respective decrease of the molar mass of the samples. However, about 10% difference in the value of β for nonsubstituted samples (with $z = 0$) from the different batches was found, which cannot be accounted for by the difference in their compositions. It also should be noted that the values of β for the $Rb_{0.8}Fe_{1.6}Se_2$ samples studied in the course of this work are close to $\beta = 1.018$ mJ mol^{-1}K^{-4} reported in Ref. [54] and $\beta = 1.1$ mJ mol^{-1}K^{-4} in Ref. [55] for $K_xFe_{2-y}Se_2$ indicating comparable lattice and magnetic contributions to the total

TABLE III. Parameters calculated from the specific heat data for $Rb_{1-x}Fe_{2-y}Se_{2-z}S_z$ samples.

Sample label	Substitution z	γ_0(0 K) mJ mol^{-1}K^{-2}	β mJ mol^{-1}K^{-4}	θ_D K	γ_n(SC) mJ mol^{-1}K^{-2}	N States/(eV f.u.)
BR19 NSC[a]	0	–	0.97(1)	215.4	–	–
BR16s1	0	0.18	1.10(1)	206.5	10.7	4.5
BR16s8	0	0.24	1.07(1)	208.4	10.7	4.5
BR26s1	0	0.09	0.99(1)	213.9	6.2	2.6
BR26s6	0	0.08	1.04(1)	210.4	7.1	3.0
BR26s11	0	0.30	1.04(1)	210.4	13.7	5.8
BR26s12	0	0.10	1.02(1)	211.8	9.8	4.2
BR26s13	0	0.09	0.98(1)	214.6	7.4	3.1
Average	0	0.15	1.02(1)	211.8	10.3	4.4
BR98	0.25	0.51	0.91(2)	220.0	5.3	2.3
BR96	0.5	0.23	0.83(1)	226.9	3.9	1.7
BR80	1.0	0.12	0.79(1)	230.6	3.5	1.5
BR87	1.0	0.25	0.78(1)	231.6	3.7	1.6
BR82	1.1	0.23	0.77(1)	232.6	1.5	0.6
BR107	1.2	0.81	0.764(6)	233.2	1.4	0.6
BR109	1.3	0.81	0.764(6)	233.2		
BR97	2.0	1.51	0.533(6)	262.9	–	

[a]NSC-nonsuperconducting sample.

specific heat despite a considerable difference (∼15%!) in the molar mass of the K and Rb- based systems. We do not have a reasonable explanation of this quite surprising similarity.

The value of the normal-state Sommerfeld coefficient γ_n for superconducting samples was calculated from the temperature dependence of the electronic specific heat assuming the constraint of entropy conservation at the onset of T_c, i.e.,

$$\int_0^{Tc} \frac{Cel}{T} dT = \int_0^{Tc} \gamma n dT.$$

The applicability of this assumption for our samples is discussed in Ref. [43], Sec. H. The calculated values of γ_n(SC) related to SC phase are given in Table III. For nonsubstituted $Rb_{0.8}Fe_{1.6}Se_2$, the values of γ_n(SC) differ significantly (by factor of two!) for samples from different batches and even for samples from the same batch. To understand the reason of this variation, we analyzed the specific heat data measured under applied magnetic fields, in which the phonon and magnetic contributions are expected to be identical to those for zero field [54]. In Fig. 19, the difference in the C values measured in zero field and a field of 9 T versus temperature is shown for several samples $Rb_{0.8}Fe_{1.6}Se_2$. For all these samples, the λ anomaly at around T_c is quite sharp and its width does not exceed 4 K, being much lower than the shift of T_c by the field of 9 T [18,54]. Importantly, the amplitude of the anomaly at T_c varies only within 15% for different samples indicating that they have rather similar values of the electronic specific heat C_{el}. This indicates that the lattice and magnetic contributions used to estimate C_{el} can create significant errors in calculation of the absolute value of γ_n(SC).

Inspection of Fig. 19 reveals the following additional features in the heat-capacity data in zero field: a pronounced tail at temperatures above T_c indicating fluctuating superconductivity and a step at temperatures between 20 and 27 K, which suggests the presence of additional density of states. It is worth mentioning that even in samples that do not show a superconducting ground state, a broad anomaly in the specific-heat difference C_{0T}-C_{9T} in the temperature range from 20 K to 40 K was observed. We assume that it can be related to nonpercolated SC states due to intrinsic (substitutional) inhomogeneities of the samples.

Under assumption that the values of C_{el} for different samples with $z = 0$ are the same and in order to minimize the errors when subtracting phonon and magnon contributions, we averaged the experimentally determined specific heat data over seven measured samples. The calculated values of the parameters for the average data are given in Table III. The value of the coefficient γ_n(SC) for the averaged data equals 10.3 mJ mol^{-1}K^{-2}. The reduced specific heat jump at T_c, $\Delta C/\gamma_n(SC)T_c$, for the averaged data was 0.79. For the sample with the lowest calculated value of $\gamma_n(SC) = 6.2$ mJ mol^{-1}K^{-2} the reduced specific jump at T_c was 1.31, which is only slightly lower than the BCS estimate of 1.43 for the weak-coupling limit. It is worth mentioning that the lowest

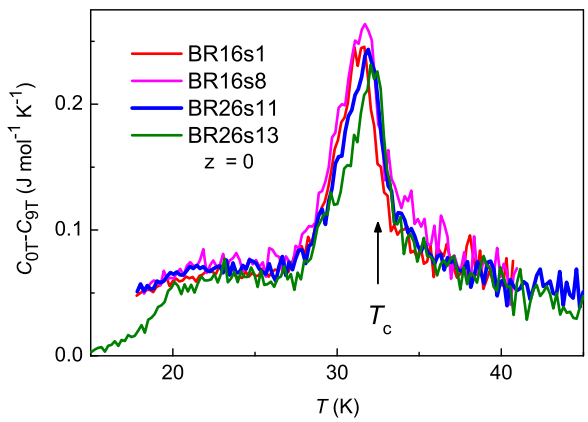

FIG. 19. Difference of the heat-capacity values measured in zero field and in an external magnetic field of 9 T *vs* temperature T for several samples of nonsubstituted $Rb_{0.8}Fe_{1.6}Se_2$($z = 0$).

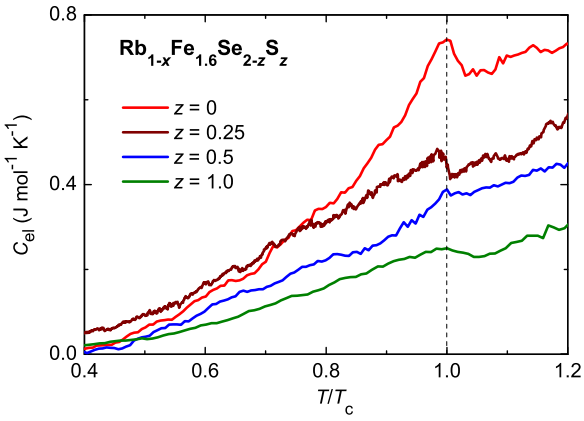

FIG. 20. Temperature dependent electronic specific heat $C_{\rm el}$ for $Rb_{1-x}Fe_{2-y}Se_{2-z}S_z$ samples with different sulfur concentration z as indicated in the figure. The dashed vertical line indicates T_c.

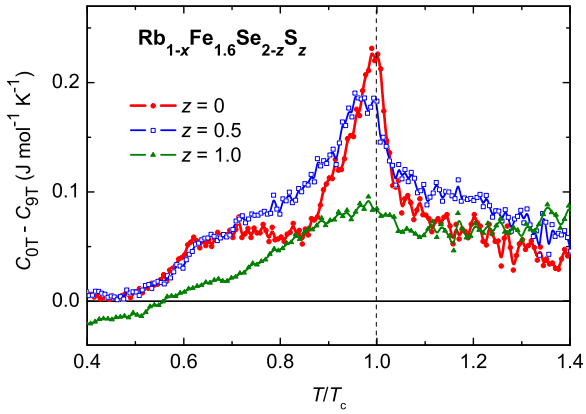

FIG. 21. Difference in the heat-capacity values measured in zero field and in field of 9 T vs temperature T for $Rb_{1-x}Fe_{2-y}Se_{2-z}S_z$ samples with different sulfur concentration z. The dashed vertical line indicates T_c.

value of $\gamma_n(\mathrm{SC}) = 6.2\,\mathrm{mJ\,mol^{-1}K^{-2}}$ obtained for our samples is close to $\gamma_n = 5.8\,\mathrm{mJ\,mol^{-1}K^{-2}}$, reported for $K_xFe_{2-y}Se_2$ by Zeng *et al.* [54]. Their value of the calculated reduced specific jump at T_c $\Delta C/\gamma_n T_c = 1.93$ is however characteristic for strong coupling. The reason of this significant difference between two related systems needs additional study. To clarify this problem, an independent method of evaluation of γ_n is desired.

Figure 20 shows the calculated electronic specific heat $C_{\rm el}$ versus temperature normalized to the critical temperature T_c for superconducting $Rb_{1-x}Fe_{2-y}Se_{2-z}S_z$ samples with different substitutions. The magnitude of the λ anomaly at T_c shows a continuous decrease with substitution indicating a reduction of the contribution from the SC quasiparticles that suggests the decrease of the amount of the minority superconducting phase. With increasing substitution, a reduction of the values of $C_{\rm el}$ and of the coefficient γ_n(SC) was derived from the experimental data. This indicates that the suppression of the superconductivity with increasing substitution is accompanied by a reduction of the density of states (DOS) at the Fermi energy. This conclusion is further supported by the data presented in Fig. 21, which shows the difference in the experimental specific heat C measured in zero field and in a field of 9 T *vs* temperature for $Rb_{1-x}Fe_{2-y}Se_{2-z}S_z$ samples with different concentrations z. With increasing z from 0 to 1.0, a significant reduction, of the magnitude of the λ anomaly in the total specific heat C at T_c estimated from the difference $C_{0\mathrm{T}}$-$C_{9\mathrm{T}}$, by a factor of 6 occurs. A somewhat smaller reduction, by a factor of 3 to 4, was estimated from the respective change of γ_n(SC) for these samples (see Table III). A better estimate of the reduction of the DOS with substitution from our data is difficult because of the uncertainty in calculating the electronic specific heat mentioned above and because of the poor statistics for samples with $z > 0$. It should also be noted that for the estimate of γ_n(SC) we applied a similar approach for all substitutions. Even if the absolute values of γ_n(SC) can be questioned, the tendency of decreasing values of γ_n(SC) with substitution is strongly supported by the data shown in Fig. 21, which represents the difference in the experimentally measured specific heats at zero and 9 T, which is independent of lattice and magnetic contributions.

It is also necessary to mention that from the Mössbauer measurements of our samples we know that the concentration of the metallic phase in the nonsubstituted samples (with $z = 0$) is about 12% [26].With increasing substitution to $z =$ 1.0, the fraction of the metallic phase increases up to 17% [46]. From the heat-capacity measurements in this work, on increasing sulfur concentration, we observed a reduction of the anomaly in the specific heat at T_c and the respective lowering of the electronic specific heat associated with the SC phase (Figs. 20 and 21). Therefore, despite the increase of the concentration of the metallic phase with increasing substitution, its contribution to the DOS related to the SC phase decreases. This suggests that only a part of the metallic phase becomes SC at low temperatures and that the relative amount of the SC phase decreases with increasing substitution.

Finally, we would like to point out that the reduction of the density of states at the Fermi energy with substitution, derived from the specific heat data is in agreement with the results of [36–38], where it was shown that with increasing substitution of S for Se, a decrease of the electronic correlations takes place. It was found that the orbital-selective Mott transition shifts to higher temperatures due to reduction of correlations in the d_{xy} channel [38], which can account for the observed suppression of T_c in the $Rb_{1-x}Fe_{2-y}Se_{2-z}S_z$ system.

G. Phase diagram and conclusions

Figure 22 presents the T-z phase diagram of $Rb_{1-x}Fe_{2-y}Se_{2-z}S_z$, which summarizes the results of our studies. At the lowest temperatures, the ground state of the samples with sulfur concentration $z \leqslant 1.2$ is superconducting coexisting with the AFM state. With increasing substitution, a nonmonotonic change of the SC transition temperature T_c takes place with an anomaly at 1/8 of substitution. The SC state disappears between concentrations 1.2 and 1.3. The AFM state is present in all samples independent on the substitution level. The AFM phase has a Fe-vacancy ordered structure below the structural transition at T_s. The transition temperature into the AFM state T_N shows a monotonous decrease indicating a weakening of AFM

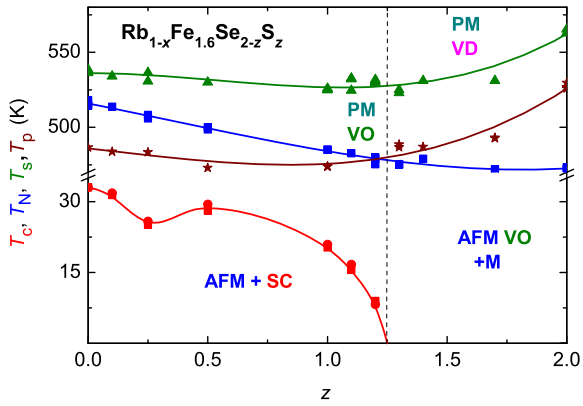

FIG. 22. T-z phase diagram of the $Rb_{1-x}Fe_{2-y}Se_{2-z}S_z$ system. SC: superconducting state, AFM VO M: antiferromagnetic vacancy ordered metallic, PM VO: paramagnetic vacancy ordered, and PM VD: paramagnetic vacancy disordered. Vertical dashed line separates SC and nonsuperconducting samples. The solid lines are drawn to guide the eye.

interactions with increasing substitution of Se by S ions. Since the AFM correlations are important for triggering the SC state via proximity effect, the weakening of the AFM interactions can contribute to the observed suppression of the superconductivity in this system. This is reminiscent of an external pressure experiment on the SC $Rb_{0.8}Fe_{1.6}Se_2$, which revealed that the suppression of the SC phase takes place concomitant with the suppression of the AFM phase [26]. A similar effect can probably take place in $Rb_{1-x}Fe_{2-y}Se_{2-z}S_z$ system due to an increase of the chemical pressure with substitution of Se by smaller S ions.

In conclusion, our detailed structural, magnetic, conductivity, and thermodynamic studies of $Rb_{1-x}Fe_{2-y}Se_{2-z}S_z$ revealed several important peculiarities of this system. The superconducting state exists up to a sulfur concentration $z = 1.2$. With increasing z, the temperature of the SC transition T_c shows a nonmonotonic drop from 32.4 K for $z = 0$ to 10 K for $z = 1.2$ with an anomaly at 1/8 of substitution. The AFM order persists in all samples of $Rb_{1-x}Fe_{2-y}Se_{2-z}S_z$ independent of substitution. With increasing concentration, the transition temperature into the AFM state T_N shows a gradual decrease from 515 K for $z = 0$ to 472 K for $z = 2$. The Fe-vacancy ordered crystal structure of the studied samples exists within the entire range of substitution. The temperature of the structural transformation into the vacancy-ordered state T_s changes nonmonotonously with substitution. It decreases from 538 K ($z = 0$) to 523 K for $z = 1.3$ and then increases again to 563 K for $z = 2$. The observed variations of the bond distances and bond angles in the Fe tetrahedrons indicate a decrease of the structural distortions with substitution.

The SC and AFM phases are coexisting in a phase-separated arrangement. For nonsubstituted samples ($z = 0$), the SC stripes are of μm size. Their composition $Rb_{0.70}Fe_{2.02}Se_2$, corresponds to a Fe-vacancy free phase. For the S-substituted samples, the phase separation of the SC and AFM phases is obviously realized on lower length scales.

Above the SC transition and below 140 K, the samples with concentrations $z \leqslant 1.2$ manifest a metallic-like conductivity, while at higher temperatures, a metal-to-semiconductor transition takes place. The ground state of the samples with substitution $z \geqslant 1.3$, including $z = 2$, is also metallic.

A significant reduction of the λ anomaly in the specific heat at the SC transition with increasing substitution indicates a reduction of the density of states at the Fermi energy that can account for the observed suppression of the superconducting state.

Finally, we would like to note that besides the above mentioned basic macroscopic results clarified by our study of the $Rb_{1-x}Fe_{2-y}Se_{2-z}S_z$ system there remains a large number of problems related to exceptional (anomalous) magnetic and conductivity behavior of several SC and non-SC samples which falls out of the general picture. Our results clearly demonstrate that the phase separation in $Rb_{1-x}Fe_{2-y}Se_{2-z}S_z$ system is distinctly different from the related K-base system and requires further study of this fascinating phenomenon. The strength of the electronic correlations is still an open issue for whole family of the intercalated iron chalcogenide superconductors. It is clear that local techniques like Mössbauer spectroscopy, NMR, neutron diffraction, ARPES, TEM, STM, μSR, etc. that probe structural and electronic properties on a microscopic level can provide necessary information and clarify these issues.

ACKNOWLEDGMENTS

This work was supported by the DFG via Transregional Research Collaboration TRR 80 (Augsburg, Munich, and Stuttgart) and by Institutional project 15.817.02.06F (Moldova).The support of the Grant for Young Researchers CSSDT 18.80012.02.10F (Moldova) is also acknowledged.

[1] E. Dagotto, The unexpected properties of alkali metal ion selenide superconductors, Rev. Mod. Phys. **85**, 849 (2013).

[2] W. Bao, Structure, magnetic order and excitations in the 245 family of Fe-based superconductors, J. Phys.: Condens. Matter **27**, 023201 (2015).

[3] M. K. Wu, P. M. Wu, Y. C. Wen, M. J. Wang, P. H. Lin, W. C. Lee, T. K. Chen, and C. C. Chang, An overview of the Fe-chalcogenide superconductors, J. Phys. D: Appl. Phys. **48**, 323001 (2015).

[4] A. Krzton-Maziopa, V. Svitlyk, E. Pomjakushina, R. Puzniak, and K. Conder, Superconductivity in alkali metal intercalated iron selenides, J. Phys.: Condens. Matter **28**, 293002 (2016).

[5] W. Bao, Q. Huang, G. F. Chen, M. A. Green, D. M. Wang, J. B. He, X. Q. Wang, and Y. Qiu, A novel large moment antiferromagnetic order in $K_{0.8}Fe_{1.6}Se_2$ superconductor, Chin. Phys. Lett. **28**, 086104 (2011).

[6] P. Dudin, D. Herriott, T. Davies, A. Krzton-Maziopa, E. Pomjakushina, K. Conder, C. Cacho, J. R. Yatea, and S. C. Speller, Imaging the local electronic and magnetic properties of intrinsically phase separated $Rb_xFe_{2-y}Se_2$ superconductor using scanning microscopy techniques, Supercond. Sci. Technol. **32**, 044005 (2019).

[7] F.-C. Hsu, J. Y. Luo, K. W. Yeh, T. K. Chen, T. W. Huang, P. M. Wu, Y.-C. Lee, Y. L. Huang, Y.-Y. Chu, D. C. Yan, and

M.-K. Wu, Superconductivity in the PbO-type structure α-FeSe, Proc. Natl. Acad. Sci. USA **105**, 14262 (2008).

[8] S. He, J. He, W. Zhang, L. Zhao, D. Liu, X. Liu, D. Mou, Y.-B. Ou, Q.-Y. Wang, Z. Li, L. Wang, Y. Peng, Y. Liu, C. Chen, L. Yu, G. Liu, X. Dong, J. Zhang, C. Chen, Z. Xu, X. Chen, X. Ma, Q. Xue, and X. J. Zhou, Phase diagram and electronic indication of high-temperature superconductivity at 65 K in single-layer FeSe films, Nat. Mater. **12**, 605 (2013).

[9] J. F. Ge, Z. L. Liu, C. H. Liu, C. L. Gao, D. Qian, Q. K. Xue, Y. Liu, and J. F. Jia, Superconductivity above 100 K in single-layer FeSe films on doped $SrTiO_3$, Nat. Mater. **14**, 285 (2015).

[10] J. Guo, S. Jin, G. Wang, S. Wang, K. Yhu, T. Zhou, M. He, and X. Chen, Superconductivity in the iron selenide $K_xFe_2Se_2$ ($0 \leqslant x \leqslant 1.0$), Phys. Rev. B **82**, 180520 (2010).

[11] A. Krzton-Maziopa, Z. Shermadini, E. Pomjakushina, V. Pomjakushin, M. Bendele, A. Amato, R. Khasanov, H. Luetkens, and K. Conder, Synthesis and crystal growth of $Cs_{0.8}(FeSe_{0.98})_2$: a new iron-based superconductor with $T_c = 27$ K, J. Phys. Condens. Matter **23**, 052203 (2011).

[12] J. J. Ying, X. F. Wang, X. G. Luo, A. F. Wang, M. Zhang, Y. J. Yan, Z. J. Xiang, R. H. Liu, P. Cheng, G. J. Ye, and X. H. Chen, Superconductivity and magnetic properties of single crystals of $K_{0.75}Fe_{1.66}Se_2$ and $Cs_{0.81}Fe_{1.61}Se_2$, Phys. Rev. B **83**, 212502 (2011).

[13] C. H. Li, B. Shen, F. Han, X. Zhu, and H. H. Wen, Transport properties and anisotropy of $Rb_{1-x}Fe_{2-y}Se_2$ single crystals, Phys. Rev. B **83**, 184521 (2011).

[14] X. G. Luo, X. F. Wang, J. J. Ying, Y. J. Yan, Z. Y. Li, M. Zhang, A F. Wang, P. Cheng, Z. J. Xiang, G. J. Ye, R. H. Liu, and X. H. Chen, Crystal structure, physical properties and superconductivity in $A_xFe_2Se_2$ single crystals, New J. Phys. **13**, 053011 (2011).

[15] Y. Mizuguchi, H. Takeya, Y. Kawasaki, T. Ozaki, S. Tsuda, T. Yamaguchi, and Y. Takano, Transport properties of the new Fe-based superconductor $K_xFe_2Se_2$ ($T_c = 33$ K), Appl. Phys. Lett. **98**, 042511 (2011).

[16] A. F. Wang, J. J. Ying, Y. J. Yan, R. H. Liu, X. G. Luo, Z. Y. Li, X. F. Wang, M. Zhang, G. J. Ye, P. Cheng, Z. J. Xiang, and X. H. Chen, Superconductivity at 32 K in single-crystalline $Rb_xFe_{2-y}Se_2$, Phys. Rev. B **83**, 060512 (2011).

[17] H. D.Wang, C. H. Dong, Z. J. Li, Q. H. Mao, S. S. Zhu, C. M. Feng, H. Q. Yuan, and M. H. Fang, Superconductivity at 32 K and anisotropy in $Tl_{0.58}Rb_{0.42}Fe_{1.72}Se_2$ crystals, Europhys. Lett. **93**, 47004 (2011).

[18] V. Tsurkan, J. Deisenhofer, A. Günther, H.-A. Krug von Nidda, S. Widmann, and A. Loidl, Anisotropic magnetism, superconductivity, and the phase diagram of $Rb_{1-x}Fe_{2-y}Se_2$, Phys. Rev. B **84**, 144520 (2011).

[19] S. Medvedev, T. M. McQueen, I. A. Troyan, T. Palasyuk, M. I. Eremets, R. J. Cava, S. Naghavi, F. Casper, V. Ksenofontov, G. Wortmann, and C. Felser, Electronic and magnetic phase diagram of β-$Fe_{1.01}Se$ with superconductivity at 36.7 K under pressure, Nat. Mater. **8**, 630 (2009).

[20] S. Margadonna, Y. Takabayashi, Y. Ohishi, Y. Mizuguchi, Y. Takano, T. Kagayama, T. Nakagawa, M. Takata, and K. Prassides, Pressure evolution of the low-temperature crystal structure and bonding of the superconductor FeSe ($T_c = 37$ K), Phys. Rev. B **80**, 064506 (2009).

[21] Y. Mizuguchi, F. Tomioka, S. Tsuda, T. Yamaguchi, and Z. Takano, Superconductivity at 27 K in tetragonal FeSe under high pressure, Appl. Phys. Lett. **93**, 152505 (2008).

[22] T. Imai, K. Ahilan, F. L. Ning, T. M. McQueen, and R. Cava, Why does Unndoped FeSe Become a High- T_c Superconductor Under Pressure? Phys. Rev. Lett. **102**, 177005 (2009).

[23] J. Guo, X.-J. Chen, J. Dai, C. Zhang, J. Guo, X. Chen, Q. Wu, D. Gu, P. Gao, L. Yang, K. Yang, X. Dai, H.-k. Mao, L. Sun, and Z. Zhao, Pressure-Driven Quantum Criticality in Iron-Selenide Superconductors, Phys. Rev. Lett. **108**, 197001 (2012).

[24] L. Sun, X.-J. Chen, J. Guo, P. Gao, Q.-Y. Huang, H. Wang, M. Fang, X. Chen, G. Chen, Q. Wu, C. Zhang, D. Gu, X. Dong, L. Wang, K. Yang, A. Li, X. Dai, H.-k. Mao, and Z. Zhao, Re-emerging superconductivity at 48 K in iron chalcogenides, Nature (London) **483**, 67 (2012).

[25] M. Gooch, B. Lv, L. Z. Deng, T. Muramatsu, J. Meen, Y. Y. Xue, B. Lorenz, and C. W. Chu, High-pressure study of superconducting and nonsuperconducting single crystals of the same nominal composition $Rb_{0.8}Fe_2Se_2$, Phys. Rev. B **84**, 184517 (2011).

[26] V. Ksenofontov, S. A. Medvedev, L. M. Schoop, G. Wortmann, T. Palasyuk, V. Tsurkan, J. Deisenhofer, A. Loidl, and C. Felser, Superconductivity and magnetism in $Rb_{0.8}Fe_{1.6}Se_2$ under pressure, Phys. Rev. B **85**, 214519 (2012).

[27] V. Svitlyk, D. Chernyshov, E. Pomjakushina, A. Krzton-Maziopa, K. Conder, V. Pomjakushin, and V. Dmitriev, Temperature and pressure evolution of the crystal structure of $A_x(Fe_{1-y}Se)_2$ (A = Cs, Rb, K) studied by synchrotron powder diffraction, Inorg. Chem. **50**, 10703 (2011).

[28] M. Bendele, C. Marini, B. Joseph, G. M. Pierantozzi, A. S. Caporale, A. Bianconi, E. Pomjakushina, K. Conder, A. Krzton-Maziopa, T. Irifune, T. Shinmei, S. Pascarelli, P. Dore, N. L. Saini, and P. Postorino, Interplay of electronis and lattice degrees of freedom in $A_{1-x}Fe_{2-y}Se_2$ superconductors under pressure, Phys. Rev. B **88**, 180506(R) (2013).

[29] P. Gao, R. Yu, L. Sun, H. Wang, Z. Wang, Q. Wu, M. Fang, G. Chen, J. Guo, C. Zhang, D. Gu, H. Tian, J. Liu, Y. Li, X. Li, S. Jiang, K. Yang, A. Li, Q. Si, and Z. Zhao, Role of the 245 phase in alkaline iron selenide superconductors revealed by high-pressure studies, Phys. Rev. B **89**, 094514 (2014).

[30] M. H. Fang, H. M. Pham, B. Qian, T. J. Liu, E. K. Vehstedt, Y. Liu, L. Spinu, and Z. Q. Mao, Superconductivity close to magnetic instability in $Fe(Se_{1-x}Te_x)_{0.82}$, Phys. Rev. B **78**, 224503 (2008).

[31] K. W. Yeh, T.-W. Huang, Y. Huang, T.-K. Chen, F.-C. Hsu, P. M. Wu, Y.-C. Lee, Y.-Y. Chu, C.-L. Chen, J.-Y. Luo, D.-C. Yan, and M.-K. Wu, Tellurium substitution effect on superconductivity of the α-phase iron selenide, Europhys. Lett. **84**, 37002 (2008).

[32] H. Lei, M. Abeykoon, E. S. Bojin, K. Wang, J. B. Warren, and C. Petrovic, Phase Diagram of $K_xFe_{2-y}Se_{2-z}S_z$ and the Suppression of its Superconducting State by an Fe2−Se/S Tetrahedron Distortion, Phys. Rev. Lett. **107**, 137002 (2011).

[33] Y. Cai, Z. Wang, Z. W. Wang, Z. A. Sun, H. X. Yang, H. F. Tian, C. Ma, B. Zhang, and J. Q. Li, Microstructural properties of $K_{0.8}Fe_{1.6}S_2$, $K_{0.8}Fe_{1.75}Se_{2-y}S_y$ ($0 \leqslant y \leqslant 2$) and $K_{0.8}Fe_{1.5+x}S_2$ ($0 \leqslant x \leqslant 0.5$) single crystals, Europhys. Lett. **103**, 37010 (2013).

[34] M. Wang, W. Tian, P. Valdivia, S. Chi, E. Bourret-Courchesne, P. Dai, and R. J. Birgeneau, Two spatially separated phases in $Rb_{0.8}Fe_{1.5}S_2$, Phys. Rev. B **90**, 125148 (2014).

[35] M. Wang, M. Yi, W. Tian, E. Bourret-Courchesne, and R. J. Birgeneau, Elucidating the magnetic and superconducting phases in the alkali metal intercalated iron chalcogenides, Phys. Rev. B **93**, 075155 (2016).

[36] M. Yi, M. Wang, A. F. Kemper, S.-K. Mo, Z. Hussain, E. Bourret-Courchesne, A. Lanzara, M. Hashimoto, D. H. Lu, Z.-X. Shen, and R. J. Birgeneau, Bandwidth and Electron Correlation-tuned Superconductivity in $Rb_{0.8}Fe_2(Se_{1-z}S_z)_2$, Phys. Rev. Lett. **115**, 256403 (2015).

[37] X. H. Niu, S. D. Chen, J. Jiang, Z. R. Ye, T. L. Yu, D. F. Xu, M. Xu, Y. Feng, Y. J. Yan, B. P. Xie, J. Zhao, D. C. Gu, L. L. Sun, Q. Mao, H. Wang, M. Fang, C. J. Zhang, J. P. Hu, Z. Sun, and D. L. Feng, A unifying phase diagram with correlation-driven superconductor-to-insulator transition for the 122* series of iron chalcogenides, Phys. Rev. B **93**, 054516 (2016).

[38] Zhe Wang, V. Tsurkan, M. Schmidt, A. Loidl, and J. Deisenhofer, Tuning orbital-selective correlations in superconducting $Rb_{0.75}Fe_{1.6}Se_{2-z}S_z$, Phys. Rev. B **93**, 104522 (2016).

[39] Zhe Wang, M. Schmidt, J. Fischer, V. Tsurkan, M. Greger, D. Vollhardt, A. Loidl, and J. Deisenhofer, Orbital-selective metal–insulator transition and gap formation above T_c in superconducting $Rb_{1-x}Fe_{2-y}Se_2$, Nature Communications **5**, 3202 (2014).

[40] G. M. Sheldrick, Crystal structure refinement with *SHELXL*, Acta Cryst. C **71**, 3 (2015).

[41] L. J. Farrugia, *WinGX* suite for small-molecule single-crystal crystallography, J. Appl. Crystallogr. **32**, 837 (1999).

[42] A. Charnukha, A. Cvitkovic, T. Prokscha, D. Propper, N. Ocelic, A. Suter, Z. Salman, E. Morenzoni, J. Deisenhofer, V. Tsurkan, A. Loidl, B. Keimer, and A. V. Boris, Nanoscale Layering of Antiferromagnetic and Superconducting Phases in $Rb_2Fe_4Se_5$ Single Crystals, Phys. Rev. Lett. **109**, 017003 (2012).

[43] See Supplemental Material at http://link.aps.org/supplemental/10.1103/PhysRevB.101.054516 for details on the microstructure of the samples, the structural refinement, structural data, differential scanning calorimetry data, a comparison of susceptibility and differential scanning calorimetry data, specific heat data, and the temperature-dependent resistivity in different applied magnetic fields in the vicinity of superconducting transition for $Rb_{1-x}Fe_{2-y}Se_{2-z}S_z$ with different z.

[44] V. Yu. Pomjakushin, A. Krzton-Maziopa, E. Pomjakushina, K. Conder, D. Chernyshov, V. Svitlyk, and A. Bosak, Intrinsic phase separation in the antiferromagnetic superconductor $Rb_xFe_{2-y}Se_2$: a diffraction study, J. Phys.: Condens. Matter **24**, 435701 (2012).

[45] Y. Texier, J. Deisenhofer, V. Tsurkan, A. Loidl, D. S. Inosov, G. Friemel, and J. Bobroff, NMR Study in the Iron-selenide $Rb_{0.74}Fe_{1.6}Se_2$: Determination of the Superconducting Phase as iron Vacancy-free $Rb_{0.3}Fe_2Se_2$, Phys. Rev. Lett. **108**, 237002 (2012).

[46] V. Ksenofontov *et al.* (unpublished).

[47] P. Zavalij, Wei Bao, X. F. Wang J. J. Ying, X. H. Chen, D. M. Wang, J. B. He, X. Q. Wang, G. F. Chen, P.-Y. Hsieh, Q. Huang, and M. A. Green, Structure of vacancy-ordered single-crystalline superconducting potassium iron selenide, Phys. Rev. B **83**, 132509 (2011).

[48] V. Yu. Pomjakushin, D. V. Sheptyakov, E. V. Pomjakushina, A. Krzton-Maziopa, K. Conder, D. Chernyshov, V. Svitlyk, and Z. Shermadini, Iron-vacancy superstructure and possible room-temperature antiferromagnetic order in superconducting $Cs_yFe_{2-x}Se_2$, Phys. Rev. B **83**, 144410 (2011).

[49] S. Weyeneth, M. Bendele, F. von Rohr, P. Dluzewski, R. Puzniak, A. Krzton-Maziopa, S. Bosma, Z. Guguchia, R. Khasanov, Z. Shermadini, A. Amato, E. Pomjakushina, K. Conder, A. Schilling, and H. Keller, Superconductivity and magnetism in $Rb_xFe_{2-y}Se_2$: Impact of thermal treatment on mesoscopic phase separation, Phys. Rev. B **86**, 134530 (2012).

[50] B. Shen, B. Zeng, G. F.Chen, J. B. He, D. M. Wang, H. Yang, and H. H. Wen, Intrinsic percolative superconductivity in $K_xFe_{2-y}Se_2$ single crystals, Europhys. Lett. **96**, 37010 (2011).

[51] D. P. Shoemaker, D. Y. Chung, H. Claus, M. C. Francisco, S. Avci, A. Llobet, and M. G. Kanatzidis, Phase relation in $K_xFe_{2-y}Se_2$ and the structure of superconducting $K_xFe_2Se_2$ via high-resolution synchrotron diffraction, Phys. Rev. B **86**, 184511 (2012).

[52] N. R. Werthamer, E. Helfand, and P. C. Hohenberg, Temperature and purity dependence of the superconducting critical field, H_{c2}. III. Electron spin and spin-orbit effects, Phys. Rev. **147**, 295 (1966).

[53] The Debye temperature is effective in a sense that it contains the magnetic contribution as well. However, since the modelled specific heat also includes a magnetic term, this does not influence the calculations of the electronic specific heat.

[54] B. Zeng, B. Shen, G. F. Chen, J. B. He, D. M. Wang, C. H. Li, and H. H. Wen, Nodeless superconductivity of single crystalline $K_xFe_{2-y}Se_2$ revealed by the low-temperature specific heat, Phys. Rev. B **83**, 144511 (2011).

[55] D. Yazici, A. C. Basaran, J. G. Ramirez, I. K. Schuller, and M. B. Maple, Structure, magnetization, specific heat, and microwave properties of $K_xFe_{2-y}Se_2$, Supercond. Sci. Technol. **29**, 085015 (2016).